Diversity and pathobiology of an ilarvirus unexpectedly detected in diverse plants and global sequencing data

Mark Paul Selda Rivarez,[1,†,*] Chantal Faure,[2] Laurence Svanella-Dumas,[2] Anja Pecman,[1] Magda Tušek-Žnidaric,[1] Deborah Schönegger,[2] Kris De Jonghe,[3] Arnaud Blouin,[4,‡], David Rasmussen[5,6], Sebastien Massart,[4] Maja Ravnikar,[1] Denis Kutnjak,[1] Armelle Marais,[2] and Thierry Candresse[2,*]

[1]Department of Biotechnology and Systems Biology, National Institute of Biology, Ljubljana, 1000, Slovenia
[2]Univ. Bordeaux, INRAE, UMR 1332 Biologie du Fruit et Pathologie, Villenave d'Ornon, 33882, France
[3]Plant Sciences Unit, Flanders Research Institute for Agriculture, Fisheries and Food, Merelbeke, 9820, Belgium
[4]Plant Pathology Laboratory, TERRA-Gembloux Agro-Bio Tech, University of Liège, Gembloux, 5030, Belgium
[†]present affiliations: [5]Department of Entomology and Plant Pathology, North Carolina State University, Raleigh, 27606, USA; [6]Bioinformatics Research Center, North Carolina State University, 27607, USA; College of Agriculture and Agri-Industries, Caraga State University, Butuan City, 8600, Philippines
[‡]present affiliation: Plant Protection Department, Agroscope, Nyon, 1260, Switzerland
*corresponding authors: M.P.S. Rivarez (mpsrivarez@gmail.com) and T. Candresse (thierry.candresse@inrae.fr)

ABSTRACT

High-throughput sequencing (HTS) and sequence mining tools revolutionized virus detection and discovery in recent years and implementing them with classical plant virology techniques results to a powerful approach to characterize viruses. An example of a virus discovered through HTS is Solanum nigrum ilarvirus 1 (SnIV1) (*Bromoviridae*), which was recently reported in various solanaceous plants from France, Slovenia, Greece, and South Africa. It was likewise detected in grapevines (Vitaceae) and several Fabaceae and Rosaceae plant species. Such very diverse set of source organisms is atypical for ilarviruses, thus warranting further investigation. In this study, modern and classical virological tools were combined to accelerate the characterization of SnIV1. Through HTS-based virome surveys, mining of sequence read archive datasets, and literature search, SnIV1 was further identified from diverse plant and non-plant sources globally. SnIV1 isolates showed relatively low variability compared to other phylogenetically related ilarviruses. Phylogenetic analyses showed a distinct basal clade of isolates from Europe, while the rest formed clades of mixed geographic origin. Furthermore, systemic infection of SnIV1 in *Solanum villosum* and its mechanical and graft transmissibility to solanaceous species were demonstrated. Near identical SnIV1 genomes from the inoculum (*S. villosum*) and inoculated *Nicotiana benthamiana* were sequenced, thus partially fulfilling Koch's postulates. SnIV1 was

shown to be seed-transmitted and potentially pollen-borne, has spherical virions, and possibly induces histopathological changes in infected *N. benthamiana* leaf tissues. Overall, this study provides information to better understand the diversity, global presence, and pathobiology of SnIV1, however, its possible emergence as a destructive pathogen remains uncertain.

Keywords: *Ilarvirus*, Solanaceae, Serratus, virus diversity, phylogenetics, histopathology, virion morphology, symptomatology, virus transmission, pollen

INTRODUCTION

The combination of classical virology techniques, modern high-throughput sequencing (HTS), and bioinformatics tools provides a powerful approach to detect, identify, and characterize viruses and monitor changes in their populations even before they emerge and cause disease outbreaks (Maclot et al. 2020; McLeish et al. 2021; Kumar et al. 2022). The COVID-19 pandemic and the persistent risks posed by plant and animal virus diseases to our food supply (Morens et al. 2020; Ristaino et al. 2021; Meurens et al. 2021) have increased interest in viromic surveys of ecosystems and data-driven virus discovery (Carroll et al. 2018; Lauber and Seitz 2022). This led to a recent surge in the discovery of viruses and other virus- or viroid-like agents from various studies (Gregory et al. 2019; Edgar et al. 2022; Mifsud et al. 2022; Zayed et al. 2022; Neri et al. 2022; Lee et al. 2023; Rivarez et al. 2023; Hou et al. 2023). As a result, hundreds of thousands of putative novel viruses remain uncharacterized due to the astounding amount of experimental work it requires. For plant virologists, this entails an immense task to uncover the biological properties of newly identified plant viruses and to systematically assess their possible economic and biosecurity risks (Massart et al. 2017; Hou et al. 2020; Rivarez et al. 2021; Fontdevila et al. 2023).

Some recent studies combined classical and modern tools and techniques to characterize recently discovered plant viruses. For instance, the biological characterization of an emerging pathogen of tomato, Physostegia chlorotic mottle alphanucleorhabdovirus (family *Rhabdoviridae*), was significantly accelerated through an international collaboration driven by HTS data (Temple et al. 2022, 2023). Recently, mining of thousands of *Arabidopsis thaliana* publicly available sequence read archive (SRA) datasets uncovered a novel comovirus (family *Secoviridae*), Arabidopsis latent virus 1, which was demonstrated to be mechanically and seed transmitted, but causes no symptoms in *A. thaliana*, (Verhoeven et al. 2023). A recent study on *Prunus*-associated luteoviruses (family *Luteoviridae*) also uncovered a new luteovirus through a search of SRA datasets (Khalili et al. 2023). Many HTS-based discoveries of crop and non-crop viruses have also been reported (Gaafar et al. 2020; Rivarez et al. 2023; Ma et al. 2019; Xu et al. 2017), but only a small subset of these studies has biologically characterized the identified viruses (Hou et al. 2020; Rivarez et al. 2021).

Among these newly discovered but marginally characterized viruses is Solanum nigrum ilarvirus 1 (SnIV1), which was recently associated with wild, weedy, or cultivated species, primarily from the Solanaceae family. SnIV1 belongs to the genus *Ilarvirus*, which is the largest genus in the family *Bromoviridae* with 22 recognized species (ICTV 2023), with some causing

significant economic losses (Rivarez et al. 2021). Ilarviruses are known to be pollen and/or seed transmitted (Mink 1993; Card et al. 2007) and their transmission was also reported to be facilitated by thrips or by pollinators (Bristow and Martin 1999). Ilarviruses pose persistent threats to fruit production such as for *Prunus* species (Pallas et al. 2012) or blackberry (*Rubus fruticosus*) (Poudel et al. 2014). In recent years, several ilarviruses were reported to cause problems in tomato in the USA, including tomato necrotic streak virus (TomNSV) (Badillo-Vargas et al. 2016; Adkins et al. 2015) and tomato necrotic spot virus (ToNSV) (Bratsch et al. 2019, 2018). Other economically important ilarviruses known to be emerging or endemic pathogens of tomato include parietaria mottle virus (PMoV) (Aparicio et al. 2018), tobacco streak virus (TSV) (Sharman et al. 2015)and spinach latent virus (SpLV) (Vargas-Asencio et al. 2013). TSV and PMoV are the closest phylogenetically-related viruses to SnIV1 (Ma et al. 2020).

SnIV1 was detected in Solanaceae crop and non-crop plants from France (*Solanum nigrum* and *S. lycopersicum*) (Ma et al. 2020), Slovenia (*Physalis* sp.) (Rivarez et al. 2023), South Africa (*S. chenopodioides*) (Mahlanza et al. 2022), and Greece (*Capsicum annuum*) (Orfanidou et al. 2022). The recent report from Greece demonstrated SnIV1 infectivity in *Nicotiana benthamiana* and *C. annuum* (Orfanidou et al. 2022). However, SnIV1 infectivity has not yet been extensively tested for the other crops and wild plants with which it has been found associated. Interestingly, SnIV1 was concurrently reported under different names [*i.e.*, grapevine-associated ilarvirus (GaIV), surrounding legume-associated ilarvirus (sLaIV), and Erysiphe necator-associated ilar-like virus 1 (EnaIV1)] in viromic studies involving plants from different botanical families. These studies detected SnIV1 sequences in association with legume (Fabaceae) plants from Germany (Gaafar et al. 2020) and grapevines (Vitaceae) from Italy and Spain (Chiapello et al. 2020, 2019). Recently, SnIV1 has also been reported from Rosaceae fruit trees such as peaches (*Prunus persica*) from the USA (Dias et al. 2022) and apricots (*Prunus armeniaca*) from South Africa (Bester and Maree 2023). Such a diverse list of source materials and potential hosts is unusual for an ilarvirus since genus members usually have host ranges limited to species of the same botanical family (Badillo-Vargas et al. 2016).

In this study, aside from modern HTS and sequence mining approaches, classical techniques such as experimental host range tests, extensive geographical surveys, histopathological observations, diversity and phylogenetic analyses, and subsequent virus detection using RT-PCR tests were implemented to characterize SnIV1. The general aim was to assess its global diversity and distribution and to characterize some of its biological properties. Specifically we aimed to answer the following questions: (1) can information on SnIV1 geographic distribution and tentative hosts be expanded using an HTS-based viromic survey of various plant species and by searching relevant SRA datasets? (2) do global isolates of SnIV1 show distinct phylogenetic clustering and what is SnIV1 level of genetic diversity compared to that of other related species such as TSV and PMoV? (3) can SnIV1 infect a range of experimental host plants and induce histopathological changes in these hosts? (4) what are the potential routes of transmission of SnIV1? Collectively, the data gathered from this study contribute to a better understanding of the

diversity and pathobiology of this little-known ilarvirus, which should aid in assessment of its risk and further spread and emergence as a destructive pathogen.

MATERIALS AND METHODS

This study is a collaborative effort involving several European partners. The majority of the experiments, including SRA mining, inoculation and other greenhouse experiments were done at INRAE, while additional inoculation experiments, nanopore sequencing, and electron microscopy were done at NIB. Separate HTS-based surveys with PCR confirmation were performed at ULiege and ILVO. The shared aim was to consolidate information on the detections of SnIV1, share genomic sequences for further analyses, and perform further biological and epidemiological characterization.

Plant samples. The following plant species were collected in the INRAE Bordeaux research Center (Villenave d'Ornon, France), tested for SnIV1 infection, and/or sequenced in the surveys of this study: (1) *Solanum villosum* that underwent Nanopore sequencing and RT-PCR testing, (2) *S. nigrum* that underwent RT-PCR testing, (3) *Vitis vinifera* cultivar (cv.) Sauvignon, (4) *V. vinifera* cv. Ugni Blanc, and (5) *Daucus carota* subspecies (subsp.) *carota* that underwent Illumina sequencing and RT-PCR testing. Samples of *S. melongena* and *S. tuberosum* were similarly obtained from selected farms in Belgium and were submitted for Illumina sequencing and underwent further RT-PCR testing. Details on how RNA was extracted and sequenced are presented below.

Following positive RT-PCR tests for SnIV1, two *S. villosum* plants were uprooted from the field, cleaned, pruned, and introduced in an insect-proof greenhouse. Two SnIV1-positive grapevine samples (*V. vinifera* cv. Sauvignon) were introduced in the same greenhouse by preparing and transplanting cleaned stem cuttings from each plant. Both samples were maintained for three months in the greenhouse before retesting for SnIV1 and utilizing them in subsequent experiments as described below.

Nucleic acid extraction methods for RT-PCR assays and Illumina-based HTS. Different methods were used for RNA extraction from field samples, greenhouse-introduced plants, or inoculated test plants prior to RT-PCR testing and/or HTS on Illumina platforms.

For total RNA extractions performed in France, a previously described method (Foissac et al. 2005) was used for leaves, stems, seeds, fruits, roots, pollen, and floral parts of *S. villosum* and for the pollen of *S. nigrum* prior to RT-PCR testing. Likewise, this protocol was used to extract total RNAs individually from inoculated test plants prior to RT-PCR testing. The Spectrum^{TM} Total Plant RNA kit (Sigma-Aldrich, Saint-Quentin-Fallavier, France) was used, following the kit instructions, to extract total RNA from grapevine leaves, petioles, bark, and phloem scrapings for RT-PCR testing. A previously described total RNA extraction protocol (Svanella-Dumas et al. 2022) was used for individual grapevine leaf tissues (for cv. Ugni Blanc) or phloem scrapings (cv. Sauvignon) prior to HTS. Double-stranded RNA (dsRNA) from 45 pools of carrot plants (50 plants each) were purified as previously described protocol (Ma et al. 2020) prior to HTS (Schönegger 2023).

Virion-associated nucleic acid (VANA) were purified from pools of 50 individual samples each for *S. melongena* and *S. tuberosum* from Belgium prior to HTS as previously described (Palanga et al. 2016; Hammond et al. 2020).

Prior to RT-PCR assays of inoculated test plants from Slovenia, RNeasy^{TM} Plant Mini Kit (Qiagen, USA) was used to extract total RNAs from all samples following the kit instructions.

RT-PCR assays. Oligonucleotide primers specific for SnIV1 RNA 3 segment or tomato betanucleorhabdovirus 2 (TBRV2, detected in mixed infection with SnIV1 in *S. villosum*) (Supplementary Table 1) were used in RT-PCR tests conducted in Slovenia using the OneStep^{TM} RT-PCR kit (Qiagen, USA) as previously described (Rivarez et al. 2023). Additional SnIV1 primers targeting RNA 1 and RNA 3 segments were designed using OligoCalc (Kibbe 2007) and used in two-step RT-PCR reactions as previously described (Marais et al. 2014) to test for SnIV1 in different plant samples from France. In each RT-PCR assay, RNA extracts from SnlV1-positive samples were used as positive control, RNA extraction control and/or healthy plants as negative controls, and no template (water only) as blank control.

Nanopore sequencing. A CTAB-based protocol (Chang et al. 1993) was used to extract total RNAs from SnIV1-infected *S. villosum* that served as inoculum and from inoculated *N. benthamiana* prior to Nanopore sequencing. Details of the nanopore sequencing methods can be found in Supplementary Materials.

Search for SnIV1 sequences in databases and the literature and assembly of SnIV1 genomes. Publicly available databases and the literature were searched for SnIV1 sequences and a previously described bioinformatic pipeline was used for the reference-guided assembly of SnIV1 genomes from HTS data in this study (Pecman et al. 2017; Rivarez et al. 2023). Details of the methods used can be found in Supplementary Materials.

Multiple sequence alignments and recombination detection analyses. To examine the molecular diversity of SnIV1, nucleotide (nt) sequences were aligned using MUSCLE (Edgar 2004) as implemented in MEGA X (Kumar et al. 2018). To compare SnIV1 diversity with that of other phylogenetically-related ilarviruses, sequences of isolates of tobacco streak virus (TSV) and Parietaria mottle virus (PMoV) were retrieved from GenBank r.v. 250 and similarly aligned .

Prior to diversity and phylogenetic analyses, possible recombination events among the SnIV1, TSV, or PMoV sequences were checked using RDP v. 5 (Martin et al. 2021). A recombination event was considered significant if it has a p-val$<10^{-4}$ in at least four of the methods used (RDP, GENECONV, Bootscan, Maxchi, Chimaera, SiSscan, PhylPro, LARD, 3Seq) (de Klerk et al. 2022; Stewart et al. 2014). Recombinant sequences were removed and unaligned ends for each genome segment of the remaining isolates manually trimmed.

Nucleotide diversity and genetic variation analyses. The coding regions of the three RNA segments of SnIV1, TSV, and PMoV were used for subsequent diversity and genetic variation analyses. The movement protein (MP) and coat protein (CP) ORFs from the RNA 3 segment of each viral isolate were concatenated into a contiguous sequence. Since most isolates have full RNA 3 sequence, their MP and CP were concatenated to achieve uniformity in length and retain coding information for all isolates, which will be useful in the subsequent analyses where nucleotide

diversity was calculated in a codon-based steps (*i.e.*, step size of 3, see description below). In this way, variable regions can be easily pinpointed to specific coding regions, not just in any random portion of the genome. The RNA 1, RNA 2, and concatenated RNA 3 alignments were then used separately to perform pairwise identity and nucleotide diversity analyses. For each genome segment, pairwise identities were calculated using SDT v. 1.2 (Muhire et al. 2014).

Genome-wide polymorphisms were detected and nucleotide diversities [pi (π)] and molecular genetic variation [theta (θ), based on π and finite sites model] (Subramanian 2016) were calculated with DnaSP v. 6 (Rozas et al. 2017) using a sliding windows of 30 bases and a step size of 3. Overall genetic distances were calculated in MEGA X (Kumar et al. 2018) using the same set of alignments. Overall π is the average probability of observing nucleotide differences at a single locus among the sequences or isolates being compared, overall θ is a measure of number of mutations or mutation rate among the sequences or isolates being compared, while overall genetic distance is the average of all pairwise genetic distances among the sequences or isolates being compared.

Phylogenetic analyses. Maximum likelihood phylogenetic analyses were used to examine the clustering of SnIV1 isolates from diverse sources. Multiple sequence alignments described above were used as input for the analyses performed in MEGA X (Kumar et al. 2018). The most suitable substitution model was selected based on the Bayesian information criteria, and the analyses were performed with 1,000 bootstrap replicates. iToL v. 6.4 (Letunic and Bork 2021) was used to visualize and annotate the resulting phylogenetic trees. Bayesian phylogeographic analysis was done in BEAST v. 2.7.4 (Bouckaert et al. 2019), as described in details in the Supplementary Materials.

Disinfection of plant tissues and seeds. To remove possible surface contaminants, including pollen grains possibly carrying SnIV1, plant tissues (including seeds) were surface disinfected prior to RNA extraction. This was done on plant samples from INRAE, France including the greenhouse-introduced *S. villosum* and grapevine (cv. Sauvignon) tissues, as well as leaves of inoculated test plants. Disinfection was done by soaking the tissues in a 5% sodium hypochlorite solution for 10 min with intermittent agitation, followed by six washes in sterile water with blot-drying in between. The sodium hypochlorite solution and water were replaced for every new tissue fragment being disinfected and washed. After the washing, disinfected plant tissues were air-dried for at least 15 min before proceeding with RNA extraction.

Preparation of floral parts and pollen for RNA extraction. Individual floral parts and pollen were tested for the presence of SnIV1. Ten flowers from the greenhouse-introduced, SnIV1-infected *S. villosum* plant (described above) were collected. Pedicels, sepals, pistils, stamens, and petals were dissected and separately pooled prior to RNA extraction.

Pollen grains were collected from the same *S. villosum* plant described above and from *S. nigrum* inoculated by approach grafting (see details below). Briefly, ripe stamens were separated from flowers and vortexed in sterile water to liberate and suspend pollen grains. Stamens were then removed, and purity and integrity of pollen grains verified under the Eclipse Ni-U (Nikon, Japan) microscope with a dark field condenser in reflection mode. Pollen grains suspended in

sterile water were briefly ground using a sterile plastic pestle suitable for 1.5 ml Eppendorf tubes before proceeding with RNA extraction.

Mechanical transmission tests. The greenhouse-introduced SnIV1-infected *S. villosum* was used as the inoculum source for the mechanical inoculations. Twenty individuals per plant species with three plants for each species kept as mock-inoculated control were used as test plants. The inoculum was prepared by homogenizing 1.0 g infected tissue with 10 ml phosphate buffer (0.02 M, pH 7.8, supplemented with 0.112 g sodium diethyldithiocarbamate trihydrate (DIECA) and 0.649 ml β-mercaptoethanol per 100 ml total volume). Activated charcoal powder (0.1 g per 10 ml inoculum) was added to the ice-cold inoculum which was then used to rub-inoculate plants using approximately 0.1 ml inoculum on the second and third youngest leaves of plants that was dusted with carborundum. Plants were maintained in an insect-proof greenhouse with temperature set at 20-24°C, with 16/8 h day/night cycle. Samples from individual plants or pooled equal amounts of uninoculated newly formed leaves from inoculated plants were tested for SnIV1 presence, up until 35 days post inoculation (dpi).

Graft transmission tests. The greenhouse-introduced, SnIV1-infected *S. villosum* was used in approach-grafting transmission experiments by using the healthy, greenhouse-grown *S. nigrum* plants as recipients (n=3). Briefly, about 2-3 cm vertical length of the epidermal-parenchymal layer was removed on one side of a young stem in both source and recipient plants. The exposed tissues were joined together and secured with a perforated adhesive tape.

For chip bud grafting, the same infected *S. villosum* plant was used to obtain 2-3 cm superficial tissue strip pieces from of a young stem, which were joined with the exposed internal tissues of a young stem of recipient *S. nigrum* plants (n=2). The joined tissues were again secured with a perforated adhesive tape. Both approach- and chip bud-grafted plants were maintained in greenhouse maintained at 20-24°C, with 16/8 h day/night cycle, before RT-PCR testing for SnIV1 at five weeks after grafting.

Seed transmission tests. Seeds were collected from a greenhouse-introduced SnIV1-infected *S. villosum* (n=73) and from two randomly selected *S. nigrum* and two *S. villosum* plants from the field (INRAE, Bordeaux, France), and surface disinfected as described above. A subsample of these seeds was also tested by RT-PCR to confirm SnIV1 infection prior to sowing. Seeds were sown in a soil tray and maintained in the greenhouse with conditions set at 20-24°C, with 16/8 h day/night cycle. RT-PCR testing of germinated seedlings for SnIV1 infection was performed at three and five weeks after sowing.

Microscopic examination of SnIV1 virions and infected leaf tissues. Leaves of the same age and size from mock-inoculated and SnIV1-infected *N. benthamiana* plants were sampled at 49 dpi. For negative staining, leaf tissue homogenates were prepared by macerating them in 1.5 ml Eppendorf tubes containing phosphate buffer (0.1 M, pH 7.0). The homogenates were applied to Formvar-coated, carbon-stabilized copper grids and negatively stained with 1% uranyl acetate (SPI Supplies, USA) in phosphate buffer (0.1 M, pH 7.0) before inspection using a Talos™ transmission electron microscope (TEM) (ThermoFisher, USA).

For preparation of thin tissue sections for light microscopy, small pieces of the same leaves used for TEM observations were fixated in 3% glutaraldehyde in phosphate buffer (0.1 M, pH 7.0) for 16 h at 4 ˚C, which was followed by post-fixation in 1% osmium tetroxide in phosphate buffer (0.1 M, pH 7.0) and embedding in Agar 100 resin (Agar Scientific, UK). Semi-thin sections (0.6 µm) were cut with a Reichert Ultracut S ultramicrotome (Leica, Germany), stained with Azure II/methylene blue, and observed with an Axioskop 2 Plus microscope (Carl Zeiss, Germany).

RESULTS

SnlV1 genome sequences obtained from HTS of different plant species. SnIV1 genomes were sequenced and assembled in four different HTS experiments. Nanopore sequencing of rRNA-depleted total RNA from *Solanum villosum* (inoculum source) and inoculated *Nicotiana benthamiana* yielded mean read depth (mrd) or average coverage ranging from 29x to 15,841x with 100% genome coverage in all three genome segments (Table 1).

Illumina sequencing of dsRNA from wild carrots sampled in France yielded near complete SnIV1 genome segments with an average coverage ranging between 94x and 1,218x for the three segments. Positive RT-PCR tests confirmed the presence of SnIV1 in the dsRNA extract of the pooled wild carrot samples.

HTS of a pool of five grapevine (cv. Sauvignon) phloem scrapings samples yielded 481 reads that mapped on SnIV1 genome segments. RT-PCR tests confirmed the presence of SnIV1 in two of the five grapevines. Illumina short read sequencing of rRNA-depleted total RNA from two grapevine (cv. Ugni Blanc) plants yielded near complete SnIV1 genomes with average coverage of 16x-60x. This detection was later confirmed by RT-PCR tests for both individual samples.

Illumina sequencing of VANAs from a pool of *S. melongena* and *S. tuberosum* samples collected in Belgium yielded partial genome of SnIV1, with only a near complete RNA 3 segment assembled from the *S. melongena* dataset. The detection of SnIV1 in pooled samples of both species was later confirmed with a positive RT-PCR test. The amplicon from *S. tuberosum* was Sanger sequenced and confirmed to be SnIV1.

RT-PCR detection of SnIV1 in different plant tissues. The presence of SnIV1 was further investigated in different tissues of SnIV1-positive *S. villosum* and grapevines (cv. Sauvignon) that were cleaned before introduced and grown for several months in the greenhouse. Three cuttings each from the two Sauvignon grapevines were sampled for bark, phloem, petiole, and newly grown leaf tissues. All tissues tested negative for SnIV1 at four and eight months post-introduction in the greenhouse (Table 2).

Disinfected tissues of one of the two asymptomatic *S. villosum* plants replanted in the greenhouse were also tested three months after introduction in the greenhouse. All *S. villosum* tissues that were surface disinfected and tested in pools (*i.e.*, leaf, stem, fruits, root, flowers, and seeds pools), as well as non-disinfected individual floral parts and pollen, tested positive for SnIV1. However, since the individual floral parts were not disinfected and ensured to be free from pollens,

detection of SnIV1 might reflect presence of the virus in these floral parts or, alternatively, presence of contaminated pollen grains.

The presence of SnIV1 was also evaluated in pollen from a graft-inoculated *S. nigrum* plant (see details below) maintained in the greenhouse and in seeds from randomly sampled wild *S. nigrum* and *S. villosum* collected from the INRAE Bordeaux research center. Pollen collected from the graft-inoculated *S. nigrum* plant tested positive for SnIV1. RT-PCR tests of surface-disinfected individual seeds revealed the presence of SnIV1 in seeds from only one of the two randomly sampled *S. nigrum* plants from the field, while seeds from two *S. villosum* plants that were similarly processed tested negative for SnIV1.

Table 1. High-throughput sequencing of plant samples collected from field surveys and those collected from transmission experiments emphasizing the detection of SnIV1 (and TBRV2) sequences and its genome assembly.

Sequencing approach / Reference for assembly and mapping methods	Source plant[a] (Family) / SRA accession no. or public repository identifier	Number of quality-screened reads (min.-max. read length)[b]	SnIV1 and TBRV2 genome mapping[c]			Consensus genome GenBank accession number[e]
			Genome segment (for SnIV1)	Number of reads mapped (mean read depth (mrd) or average coverage[d])	Percent of genome covered	
Nanopore sequencing of rRNA-dep totRNA[f] / (Pecman et al. 2022)	*Solanum villosum**,#,g (Solanaceae) / SRR21292491	113,093 (100-6,769 nt)	RNA 1	167 (38x)	100.0	OP561316
			RNA 2	106 (29x)	100.0	OP561317
			RNA 3	1,287 (380x)	100.0	OP561318(12)
			TBRV2	424 (21x)	100.0	OP441765
	*Nicotiana benthamiana**,#,h (Solanaceae) / SRR21292490	183,605 (100-4,702 nt)	RNA 1	5,687 (933x)	100.0	OP561319
			RNA 2	1,449 (317x)	100.0	OP561320
			RNA 3	64,256 (15,841x)	100.0	OP561321(13)
			TBRV2	859 (31x)	100.0	OP441766
Illumina sequencing of rRNA-dep totRNA[f] / (Svanella-Dumas et al. 2022)	*Vitis vinifera* cv. Sauvignon*,g (Vitaceae) / doi:10.57745/ZIXT4A	144,803,940 (100-150 nt)	RNA 1	179 (9,6x)	72.0	(–)
			RNA 2	74 (7x)	56.0	(–)
			RNA 3	228 (11,4x)	66.0	(–)
			TBRV2	(–)	(–)	(–)
	Vitis vinifera cv. Ugni Blanc*,g (Vitaceae) plant 1 / doi:10.57745/ZIXT4A	41,648,925 (60-150 nt)	RNA 1	564 (20x)	98.6	(–)
			RNA 2	362 (16x)	97.4	(–)
			RNA 3	410 (23x)	96.6	OP561325(7)
			TBRV2	0	0	(–)
	Vitis vinifera cv. Ugni Blanc*,g (Vitaceae) plant 2 / doi:10.57745/ZIXT4A	46,064,375 (60-150 nt)	RNA 1	900 (34x)	98.2	OP561326
			RNA 2	854 (41x)	99.0	OP561327
			RNA 3	1,008 (60x)	98.4	OP561328(6)
			TBRV2	0	0	(–)
	Daucus carota subsp. *carota*g,j	9,823,623 (100-114 nt)	RNA 1	5,270 (172x)	97.4	OP561322
			RNA 2	2,314 (94x)	94.7	OP561323

Illumina sequencing of dsRNA[i] / (Schönegger 2023)	(Apiaceae) / doi:10.57745/ZIXT4A		RNA 3	24,549 (1,218x)	99.0	OP561324(8)
			TBRV2	0	0	(–)
Illumina sequencing of VANA[k] / (Buzkan et al. 2019)	*Solanum melongena**,g,j (Solanaceae) / SRR21292489	2,441,462 (150 nt)	RNA 1	357 (16x)	86.2	(–)
			RNA 2	70 (4x)	42.4	(–)
			RNA 3	887 (59x)	96.7	OP561329(2)
			TBRV2	0	0	(–)
	*Solanum tuberosum**,g,j (Solanaceae) / dataset not deposited	8,599,952 (150 nt)	RNA 1	not assembled	(–)	(–)
			RNA 2	not assembled	(–)	(–)
			RNA 3	54 (4x)	26.3	OP967014[l]
			TBRV2	0	0	(–)

(–) Sequence was not deposited because only partial or fragmented genome was assembled or the typical open reading frames were not found or are problematic or indicating that information is not available

[a] High-throughput sequencing detections confirmed by RT-PCR in individual plants are marked by an asterisk (*) for SnIV1 and hashtag (#) for TBRV2

[b] Number of valid reads after quality screening and trimming of barcodes. The number in parentheses represent the range of read length in number of nucleotides

[c] One of the SnIV1 genomes in GenBank (a.n. OL472060-OL472062) and TBRV2 genome (a.n. OL472116) were used in reference-based genome assembly in CLC-GWB, with at least 90% identity and coverage threshold. These genomes were also used to determine the percentage of genome (or genome segment) covered by the mapping

[d] On average, number of times each locus in a reference genome is covered by the mapped reads

[e] Accession numbers deposited in GenBank as third-party annotations (TPA), with number superscripts in parentheses corresponding to each SnIV1 RNA3 genome segment that were used in the phylogenetic tree construction for Fig. 1 and Supplementary Fig. 2C

[f] ribosomal RNA-depleted total RNA

[g] Samples collected from the field or greenhouse-introduced

[h] This is from a 33 dpi sample of an individual plant that was mechanically inoculated with infected tissues from greenhouse-introduced *S. villosum*

[i] double-stranded RNA

[j] This consists of 50 plants of the same species pooled into one composite sample, prior to dsRNA extraction.

[k] virion-associated nucleic acid

[l] sequenced amplicon from the RT-PCR detection of SnIV1 in a composite *S. tuberosum* sample from Belgium

Table 2. RT-PCR detection of SnIV1 in different tissues from greenhouse-introduced plants or from plants growing in the field.

Place of collection or sample description	Plant species	Plant tissue	No. of SnIV1(+) / No. of samples tested
Greenhouse-introduced or greenhouse-grown plants	*Vitis vinifera* cv. Sauvignon[a]	leaves (plant 1)	0 / 3
		petioles (plant 1)	0 / 3
		bark (plant 1)	0 / 3
		phloem (plant 1)	0 / 3
		leaves (plant 2)	0 / 3
		petioles (plant 2)	0 / 3
		bark (plant 2)	0 / 3
		phloem (plant 2)	0 / 3
	Solanum villosum[b]	leaves	4 / 4
		stems	5 / 5
		fruits	4 / 4
		roots	1 / 1
		flowers	1 / 1
		pedicels	1 / 1
		sepals	1 / 1
		pistils	1 / 1
		stamens	1 / 1
		petals	1 / 1
		seeds	8 / 10
		pollen[c] (plant 1)	1 / 1
		pollen[c] (plant 2)	1 / 1
	Solanum nigrum[d]	pollen	1 / 1
Field (growing in the wild)	*S. nigrum*	seeds (plant 1)	5 / 10
		seeds (plant 2)	0 / 10
	S. villosum	seeds (plant 1)	0 / 10
		seeds (plant 2)	0 / 10

[a] This represents testing of cuttings from two SnIV1-positive plants introduced as eight stem cuttings each in the greenhouse and tested four and eight months after transplanting.
[b] This represents results from a single SnIV1(+) plant introduced in the greenhouse and tested three months after. This plant also tested positive for tomato betanucleorhabdovirus 2 (TBRV2). Multiple samples from *S. villosum* represent tissues that were collected in different parts , *i.e.,* older stems/leaves, younger stems/leaves, and so on.
[c] Pollen was collected from the two *S. villosum* plants maintained in the greenhouse and tested separately.
[d] This plant is one of the three approach-graft inoculated plants and which tested positive for SnIV1.

***In silico* detection of SnIV1 in databases and in the literature**. Information on sequences and existing records of SnIV1 were collected to gain a comprehensive picture of its global diversity and geographic distribution (Table 3 and Supplementary Table 2). Aside from SnIV1 genomes deposited in GenBank database r.v. 250, SnlV1 was also detected through BLASTn homology searches in a publicly available transcriptome shotgut assembly (TSA) of hop (*Humulus lupulus* var. *lupulus*, family Cannabaceae) from Japan (Natsume et al. 2015). So far, this is the only detection of SnIV1 sequences that are linked to samples from Asia with dataset deposited in GenBank database. Furthermore, search of SRA datasets through palmID in Serratus (Edgar et al. 2022) returned 80 datasets with RdRp 'palmprint' sequences that are 100% identical to that of SnIV1 (103 amino acid residues, E-value < 10^{-74}). These results included detections of SnIV1 in sequence datasets from China and the USA and several European countries.

A literature search identified recent studies that detected SnIV1 sequences that were not yet available in GenBank r.v. 250 at the time of writing. This search identified four new plant viromic or disease etiology studies, including two that detected the virus in South Africa, which represent the first reports of SnIV1 in the African continent (Mahlanza et al. 2022; Bester and Maree 2023). The other two studies are viromic studies of peach in the USA (Dias et al. 2022), and an HTS study of symptomatic peppers (hybrid Arlequin F1) from Greece (Orfanidou et al. 2022). The study from Greece demonstrated the mechanical transmissibility and infectivity of SnIV1 in *N. benthamiana* and in the same genotype of peppers.

In total, 25 independent studies that detected SnIV1 sequences were identified, 15 of which were gathered through the palmID search. In terms of timing, the oldest SRA dataset with SnIV1 presence was released in 2013, and is a transcriptomic study of *Medicago trunculata* root nodules from France (Roux et al. 2014), while the most recent study concerns the viromic exploration of wild *Solanum* species (Mahlanza et al. 2022) and apricots (*P. armeniaca*) (Bester and Maree 2023) in South Africa. The geographic origin of the biological samples from these studies spanned five out of the six habitable continents or 11 countries, including eight independent studies conducted in the USA. Seventeen studies involved sequencing of plant samples, including seven that involved sequencing of members of Solanaceae family. Of the seven studies that utilized non-plant samples, four involved the sequencing of bee species (Apidae). These *in silico* searches highlighted associations of SnIV1 with 12 different plant species of economic importance (*e.g.*, crop, medicinal, ornamental, or fuel feedstock), six non-crop or wild plant species, and five animal species.

SnIV1 genomes assembled from global SRA datasets. SnIV1 genomic sequences were also assembled from representative SRA datasets identified above. In this effort, only a small subset of the 80 palmID search hits were used, with the assumption that SnIV1 isolates are possibly not significantly diverse within a single study that analyzed samples collected in the same year and country, by the same research team. SnIV1 genome segments were reconstructed by reference-guided assembly yielding average coverages ranging from 4x to 77,350x. In total, 59 of the 63 genome segments (representing 21 isolates) were successfully reconstructed and deposited in GenBank.

Table 3. SnIV1 genome assembly from selected publicly available global sequencing data.

Associated literature[a]	Sequencing data accession number (Year released)	Number of quality-screened reads (average read length)[b]	SnIV1 genome mapping[c]			GenBank accession number[e]
			Genome segment	Number of reads mapped (mean read depth (mrd) or average coverage[d])	Genome covered (%)	
(Howe et al. 2023)	SRR10849159 (2020)	156,095,145 (148 nt)	RNA 1	4,323 (188x)	99.7	BK061616
			RNA 2	2,986 (157x)	99.9	BK061617
			RNA 3	3,639 (240x)	99.8	BK061618[(23)]
	SRR10376303 (2020)	119,872,896 (147 nt)	RNA 1	3,154 (136x)	99.8	BK061619
			RNA 2	2,071 (108x)	99.9	BK061620
			RNA 3	4,709 (308x)	99.9	BK061621[(30)]
	SRR10849156 (2017)	188,311,868 (149 nt)	RNA 1	12,127 (527x)	99.9	BK061622
			RNA 2	7,173 (378x)	100.0	BK061623
			RNA 3	10,526 (694x)	100.0	BK061624[(31)]
(Mahlanza et al. 2022)	SRR15040766 (2021)	40,658,793 (150 nt)	RNA 1	648 (28x)	98.9	BK061666
			RNA 2	360 (19x)	98.3	BK061667
			RNA 3	480 (31x)	100.0	BK061668[(17)]
(Tauber et al. 2022)	SRR12659856 (2020)	72,394,575 (149 nt)	RNA 1	185 (8x)	98.8	BK061649
			RNA 2	297 (16x)	97.6	BK061650
			RNA 3	341 (23x)	99.6	BK061651[(32)]
(Sproviero et al. 2021)	SRR12387953 (2020)	57,174,266 (76 nt)	RNA 1	3,650 (80x)	99.7	BK061652
			RNA 2	3,015 (80x)	99.8	BK061653
			RNA 3	2,301 (77x)	99.6	BK061654[(27)]
(Auber et al. 2020)	SRR10758312 (2020)	32,532,748 (149 nt)	RNA 1	174,712 (7,584x)	100.0	BK061625
			RNA 2	223,487 (11,767x)	100.0	BK061626
			RNA 3	1,173,869 (77,350x)	100.0	BK061627[(33)]
	SRR10758313 (2020)	17,066,352 (150 nt)	RNA 1	174,375 (7,570x)	100.0	BK061628
			RNA 2	221,302 (11,653x)	100.0	BK061629
			RNA 3	1,169,597 (77,074x)	100.0	BK061630[(34)]
(Coady et al. 2020)	SRR11680723 (2020)	23,780,022 (141 nt)	RNA 1	5,711 (201x)	99.7	BK061655
			RNA 2	4,318 (188x)	99.5	BK061656
			RNA 3	2,459 (132x)	99.6	BK061657[(24)]
(Costa et al. 2020)	SRR11881307 (2020)	65,632,030 (98 nt)	RNA 1	167 (5x)	93.8	(–)
			RNA 2	98 (3x)	87.5	(–)
			RNA 3	122 (5x)	92.5	BK061658
(Chiapello et al. 2020)	SRR9995129[f] (2019)	44,182,895 (101 nt)	RNA 1	1,528 (43x)	98.8	BK061610
			RNA 2	1,220 (42x)	98.2	BK061611
			RNA 3	1,410 (60x)	98.9	BK061612[(21)]
	SRR11364885[f] (2020)	139,040,256 (98 nt)	RNA 1	3,100 (91x)	99.7	BK061613
			RNA 2	2,451 (87x)	99.6	BK061614
			RNA 3	2,542 (126x)	99.5	BK061615[(20)]
(Deboutte et al. 2020)	SRR10418310 (2019)	11,239,438 (113 nt)	RNA 1	4,327 (153x)	99.8	BK061659
			RNA 2	4,346 (189x)	97.1	BK061660

			RNA 3	12,796 (675x)	99.6	BK061661[(1)]
(Arnoux 2019)	ERR2576961 (2018)	29,364,317 (97 nt)	RNA 1	3,947 (112x)	98.9	BK061631
			RNA 2	1,672 (57x)	98.4	BK061632
			RNA 3	8,478 (361x)	100.0	BK061633[(18)]
(Wu et al. 2018)	SRR5380917 (2017)	12,751,998 (99 nt)	RNA 1	15,372 (441x)	100.0	BK061634
			RNA 2	6,581 (229x)	99.7	BK061635
			RNA 3	13,301 (577x)	99.8	BK061636[(28)]
	SRR5380918 (2017)	11,644,036 (98 nt)	RNA 1	593 (18x)	99.3	BK061637
			RNA 2	264 (9x)	99.5	BK061638
			RNA 3	641 (28x)	99.3	BK061639[(29)]
(Rai et al. 2018)	SRR6799516 (2018)	7,540,310 (99 nt)	RNA 1	206 (6x)	98.1	BK061640
			RNA 2	351 (12x)	98.2	BK061641
			RNA 3	3,178 (138x)	99.6	BK061642[(19)]
(Ledón-Rettig et al. 2017)	SRR4412518 (2016)	3,851,029 (75 nt)	RNA 1	476 (10x)	97.8	(–)
			RNA 2	298 (8x)	96.8	(–)
			RNA 3	205 (7x)	94.3	BK061662
(Chen et al. 2016)	SRR6387685 (2017)	39,742,426 (125 nt)	RNA 1	1,255 (46x)	99.9	BK061643
			RNA 2	1,569 (69x)	99.9	BK061644
			RNA 3	2,850 (157x)	99.8	BK061645[(14)]
(Vannette et al. 2015)	SRR1239309 (2014)	44,453,630 (96 nt)	RNA 1	227 (6x)	99.9	BK061663
			RNA 2	254 (9x)	99.7	BK061664
			RNA 3	105 (4x)	97.3	BK061665
(Roux et al. 2014)	SRR949232 (2013)	99,084,402 (47 nt)	RNA 1	5,038 (73x)	99.9	BK061646
			RNA 2	6,330 (111x)	99.7	BK061647
			RNA 3	2,060 (45x)	98.7	BK061648[(9)]

(–) Sequence was not deposited because partial or fragmented genome was assembled, or the typical open reading frames were not found or problematic.

[a] Details of the sequencing metadata from each study can be found in Supplementary Table 2.

[b] Number of reads after quality screening and trimming of barcodes. The number in parentheses represent the average read length in number of nucleotides.

[c] One of the SnIV1 genomes from GenBank (a.n. OL472060-OL472062) was used in reference-based genome assembly in CLC-GWB, with at least 90% identity and coverage threshold for reads mapping.

[d] On average, number of times each locus in a reference genome is covered by the mapped reads.

[e] Accession numbers deposited in GenBank as TPA with number superscripts in parentheses corresponding to each SnIV1 RNA 3 genome segment that were used in the phylogenetic analyses with the resulting tree shown in Fig. 1 and Supplementary Fig. 2C.

[f] Genomes assembled from the two SRA datasets (SRR9995129, SRR11364885) and another dataset (SRR9995131) that was used to assemble SnIV1 isolate DMG 25 (MN520742-MN520744, deposited with the name ‘grapevine associated ilarvirus (GaIV)’) came from the same study (Chiapello et al. 2020). However, these genomes are not 100% identical in all segments (see Supplementary Fig. 1), and thus, can be considered as three different isolates.

Phylogenetic clustering and pairwise identity comparisons of SnIV1 global isolates. No recombination was detected in the alignment of concatenated MP and CP ORFs (RNA 3 segment), thus this was used to reconstruct a maximum likelihood phylogenetic tree of the global isolates of SnIV1 (Fig. 1). Four major clades or lineages were observed, including two distinct basal lineages: one comprised of four isolates from Belgium [n=2; from eggplant (a.n. OP561329) and from honeybees (a.n. BK061661)], Germany [n=1, from a Fabaceae weed (a.n. MN412727)], and Greece [n=1, from pepper (a.n. OP066716)], forming a monophyletic clade with 99% bootstrap support (b.s.), and the other basal lineage consisted of a single isolate from Slovenia [from *Physalis* sp. (a.n. OL472062)]. Isolates from elsewhere in the world collectively formed a poorly supported clade (60% b.s.) with the Slovenian isolate as the basal lineage. The rest of the isolates formed phylogenetic clusters of mixed country or continental origin. However, Bayesian phylogeographic analysis resulted in uniformly low probabilities for all ancestral locations near the root (Supplementary Fig. 2), reflecting a high degree of uncertainty surrounding the geographic origin of SnIV1.

In terms of percent pairwise nt identity based on concatenated MP-CP ORFs (RNA 3), isolates of the basal European lineages are 94.5-96.6% identical to other isolates, while the rest of the isolates are 96.2-100% identical to each other (Supplementary Fig. 1). When the other genome segments are analyzed, isolates of the basal European lineage (Belgian, Greek, and German isolates only) are only 90.8-92.2% identical to the rest of the isolates using RNA 1 (methyltransferase-helicase (ORF 1a)), and 92.1-93.3% identical when using RNA 2 (RdRp and viral suppressor of RNA silencing (VSR) proteins (ORFs 2a and 2b)). Likewise, patterns of phylogenetic clustering similar to that of RNA 3 phylogenetic tree were observed in the RNA 1 and RNA 2 phylogenetic trees with the distinct basal lineage of European origin.

Diversity of SnIV1 compared to closely related ilarviruses. The Recombination-free alignments of SnIV1 isolates and isolates of its two phylogenetically closest species (TSV with wide host range and PMoV with narrow host range) were used to perform comparative diversity analyses (Fig. 2A-C). It is worthwhile to note that the number of available sequences varies among the three species. TSV has the highest number of sequences across the three genome segments, closely followed by SnIV1, while PMoV has the least number of sequences available. Inspection of π (nucleotide diversity) along the coding regions of each genome segment indicated that SnIV1 populations generally have lower π when compared to TSV, which has the highest overall π in any genome segment even though they have comparable number of isolates. This is obvious when examining genome-wide π for RNA 2. For TSV and PMoV, π values reach up to 27-37% probability of observing nucleotide differences at a single locus for any pairwise sequence comparison. However, highest π values for any segment of SnIV1 are around 0.11 only (or 11% probability of observing single nt differences). When overall π, as well as molecular genetic diversity (θ) and overall genetic distance were compared among the three viruses, TSV stood out with the highest values in all three segments when compared to that of both PMoV and SnIV1 (Fig. 2D).

Fig. 1. Phylogenetic clustering, source materials or organism(s), and geographical origins of 34 SnIV1 global isolates. The mid-point rooted maximum likelihood phylogenetic tree was constructed based on a multiple sequence alignment of concatenated full coding nucleotide sequences of the movement and coat proteins (RNA 3 segment). The substitution model used was Tamura 3-parameter with discrete Gamma distribution with 5 rate categories and by assuming that a certain fraction of sites is evolutionarily invariable. The tree topology shown was inferred after 1000 bootstrap replicates. Tree nodes/tips are numbered to refer to the accession numbers of SnIV1 genome sequences indicated in Supplementary Fig. 1C, with their GenBank accession numbers and metadata in Supplementary Table 2 (indicated as the same number superscripts). Isolates with experimentally-verified hosts are indicated with an asterisk (*). The world map was created using MapChart (www.mapchart.net) under the CC BY-SA 4.0 license, and icons were downloaded from PhyloPic (www.phylopic.org) under the Public Domain, CC0 or CC BY-NC 3.0 licenses.

Fig. 2. Comparative diversity analyses of global isolates of SnIV1 with those of two closely related ilarviruses, tobacco streak virus (TSV) with a known wide range of associated hosts, and Parietaria mottle virus (PMoV) with a known narrow range of associated hosts. **A-C**, Nucleotide diversity (π) calculated in window size of 30 and step of 3 nucleotides along (A) RNA 1, (B) RNA 2, and (C) RNA 3 genome segments of TSV, PMoV, and SnIV1. **D**, measures of overall π, molecular genetic variation (θ), and overall genetic distance in all genome segments of TSV, PMoV, and SnIV1. Note: $^{\#}$position in the SnIV1 alignment. *viral suppressor of RNA silencing protein.

Transmission and experimental host range of SnIV1. Approach and chip-bud grafting experiments demonstrated that SnIV1 can be transmitted through these methods from *S. villosum* to healthy *S. nigrum* plants. Newly formed leaves of plants inoculated by both grafting methods developed symptoms such as mild vein yellowing and slight leaf crinkling (Fig. 3F,G) and tested positive for SnIV1 at 18 and 27 dpi (Table 4).

Eight plant species were mechanically inoculated, seven of which are Solanaceae members, including two cultivars of *S. lycopersicum*. Three solanaceous species (*N. benthamiana, N. occidentalis,* and *S. nigrum*) developed symptoms in their newly formed, uninoculated leaves and were tested positive for SnIV1 at 28 and 35 dpi. The rest of the mechanically inoculated plant species tested negative up to 35 dpi. Symptomatic *N. benthamiana* and *N. occidentalis* plants showed general stunting and smaller, crinkled, and chlorotic leaves compared to mock inoculated plants (Fig. 3A,B), while symptomatic *S. nigrum* plants showed only subtle interveinal chlorosis in their newly formed uninoculated leaves (Fig. 3E), which tested positive for SnIV1 at around 18 and 28 dpi. *N. benthamiana* plants infected with SnIV1 later developed more deformed leaves with interveinal yellowing (Fig. 3C).

SnIV1-infected *N. benthamiana,* and *N. occidentalis,* were later determined to be co-infected with TBRV2 by nanopore sequencing. Full genome sequences of TBRV2 were recovered from the inoculum source (*S. villosum*) and inoculated *N. benthamiana* plants. These two near-identical

sequences are 90-95% identical to TBRV2 genomes deposited in GenBank from a previous study (Rivarez et al. 2023). This is the first detection of TBRV2 in a wild *S. villosum* plant and in France. However, TBRV2 was not identified from the HTS datasets of the other sequenced samples discussed above.

A single infection of SnIV1 in a *N. benthamiana* plant was observed in a separate mechanical inoculation experiment, where the plants showed distinct bending of stems at around 28 dpi and severely crumpled leaves persisting until around 105 dpi (Fig. 3D).

Possible transmission of SnIV1 from infected seeds to newly germinated young plants was demonstrated. Seedlings of both *S. villosum* and *S. nigrum*, tested in pools of 10 leaves from different plants tested positive for SnIV1 at 34 days after sowing.

Histopathology of SnIV1-infected *Nicotiana benthamiana* and SnIV1 virion morphology. Tissues of singly infected *N. benthamiana* collected at 49 dpi (plant shown in Fig. 3D at 105 dpi) were examined in comparison to those of mock-inoculated plants of the same age grown under the same conditions. In healthy tissues, normal epidermal and parenchymal cells and vascular tissues were observed (Fig. 4A-C), while SnIV1-infected tissues and cells were strikingly distorted (Fig. 4D-F). While no viral particles could be observed when ultra-thin sections were examined by TEM, a high number of viral particles were readily observed on leaf dip grids with negative staining prepared using extracts from the same *N. benthamiana* leaf (Fig. 4G-H). The virions observed were spherical and measurements performed on 70 virions yielded an average diameter of 27.6 nm, with a standard deviation of 0.6 nm. Such morphological properties are consistent with those of some ilarviruses, although for some members of the genus, unstable particles or particles of slightly different sizes or with a bacilliform shape were also reported (Simkovich et al. 2021; Adams and Antoniw 2006).

Table 4. RT-PCR detection of SnIV1 and TBRV2 in plant samples from the mechanical, seed, and graft transmission experiments.

Mode of transmission	Plant species and cultivar (if known)	Symptoms observed in newly formed leaves	Individual or pooled samples?[a]	dpi or das[b]	No. of SnIV1(+) / No. of samples tested	No. of TBRV2(+) / No. of samples tested
Mechanical[c]	*Chenopodium quinoa*	asymptomatic	pooled[f] (4)	20	0 / 4	0 / 4
	Capsicum annuum	asymptomatic	pooled[e] (5)	14	0 / 2	(–)
		asymptomatic	individual[f]	20	0 / 15	0 / 1[#]
	Nicotiana benthamiana	chlorosis and crinkling[d]	individual[e]	28	22 / 22	21 / 22
			pooled[f] (5)	18	4 / 4	(–)
			individual[g]	35	1[h] / 2	1[i] / 2
	Nicotiana glutinosa	asymptomatic	pooled (5)	14	0 / 2	(–)
	Nicotiana occidentalis	vein yellowing, necrotic spots[d]	individual[e]	28	10 / 10	(–)
			pooled[f] (5)	18	4 / 4	4 / 4
	Nicotiana tabacum cv. Xanthi	asymptomatic	pooled (5)	14	0 / 2	(–)
	Solanum lycopersicum cv. M82	asymptomatic	pooled (4)	20	0 / 4	0 / 4
	S. lycopersicum cv. Rudgers	asymptomatic	pooled (4)	20	0 / 4	0 / 4
	Solanum nigrum	vein yellowing, slight crinkling	individual[e]	28	1 / 1	(–)
			pooled[f] (5)	18	4 / 4	4 / 4
Seed[c]	*Solanum villosum*	asymptomatic	pooled (10)	34	5 / 5	(–)
	S. nigrum	asymptomatic	pooled (10)	34	7 / 7	(–)
Graft[c]	*S. nigrum* (approach grafted)	vein yellowing, slight crinkling	individual	27	2 / 2	(–)
	S. nigrum (chip bud grafted)		individual	27	3 / 3	(–)

(–) not tested

[a] Numbers enclosed in parentheses () indicate the number of plants that were pooled, prior to RNA extraction, to constitute the composite/pooled samples that were tested in RT-PCR

[b] The number indicates the last time point in which RT-PCR testing was done in days post-inoculation (dpi) for inoculated plants or days after sowing (das) for seed transmission experiment

[c] Newly formed or uninoculated young leaves were tested in these experiments

[d] general stunting was observed in this inoculated plant species

[e] first experiment

[f] second experiment

[g] third experiment

[h] This plant is TBRV2 negative, thus represent single infection of SnIV1

[i] This plant is SnIV1 negative, thus represent single infection of TBRV2

[#] Test for TBRV2 was done in a pool of all the 15 samples collected

Fig. 3. Symptoms observed in inoculated plants. **A**, mock- and mechanically inoculated *Nicotiana benthamiana* plants at 28 days post-inoculation (dpi). **B**, mock- and mechanically inoculated *N. occidentalis* plants at 28 dpi. **C**, mechanically-inoculated symptomatic *N. benthamiana* at 47 dpi. **D**, mechanically-inoculated symptomatic *N. benthamiana* at 105 dpi that was confirmed to be singly infected by SnIV1. **E**, mock- and mechanically inoculated *Solanum nigrum* plants at 35 dpi. **F**, graft-inoculated *S. nigrum* plants at 35 dpi. **G**, chip bud graft-inoculated *S. nigrum* plants at 35 dpi. Red arrows indicate distinct symptomatic parts of each plant shown. Inoculated plants shown in A and B were tested positive for TBRV2, but the rest of the plants shown did not undergo similar test for TBRV2.

Fig. 4. SnIV1-infected tissues and virions from mechanically inoculated *Nicotiana benthamiana* leaves. **A-C**, Thin sections of mock-inoculated *N. benthamiana* leaves for comparison that were taken at different magnifications under light microscope. **D-F**, Thin sections of SnIV1-inoculated *N. benthamiana* leaves that were taken at different magnifications under light microscope. Arrows indicate the nuclei (blue arrows) and chloroplasts (red arrows). **G-H**, Transmission electron micrograph of SnIV1 spherical virions from a crude preparation of mechanically-inoculated *N. benthamiana* tissues, shown at 100 nm and 50 nm scales.

DISCUSSION

Collectively, we generated novel information on the global distribution of SnIV1, its genomic diversity compared to other ilarviruses, and phylogenetic relationships among SnIV1 isolates. We also generated new information on the biology and epidemiology of SnIV1, including its infectivity in various solanaceous plants and possible transmission through seeds and pollen. These results contributed to a better understanding of SnIV1's possible propensity to emerge as a global crop pathogen.

Expansion of possible hosts and geographic distribution of SnIV1. HTS-based virome surveys implemented in this study uncovered association of SnIV1 with a new set of plant species from France and Belgium. Virome surveys conducted in Belgium detected SnIV1 in *S. melongena* and *S. tuberosum*, which are first detections of the virus in such species and in Belgium. This further expanded the number of Solanaceae species that are possible but still experimentally unverified hosts of SnIV1, a list that includes both cultivated (*i.e.*, *S. lycopersicum*) or wild species (*i.e.*, *S. chenopodioides*, *Physalis* sp.). The expanded association of solanaceous plants with SnIV1 fits very well with the results of the transmission experiments in this study, where infectivity of SnIV1 was confirmed in several solanaceous plants.

In silico and literature searches implemented here likewise contributed additional information on diverse source materials and possible hosts of SnIV1, especially those that were sampled in countries outside of Europe. Most of the plant-derived sequencing datasets with SnIV1 sequences were obtained from metagenomic or metatranscriptomic sequencing of leaf tissues of plants from different families. Interestingly, SnIV1 was detected in the metatranscriptomic sequencing of belowground parts of Fabaceae species (*Medicago*

truncatula and *Arachis hypogaea*) (Roux et al. 2014; Chen et al. 2016) and in *Lithospermum erythrorhizon* roots (Auber et al. 2020). The HTS of *L. erythrorhizon* has the highest number of SnIV1 reads among all the datasets. In the present study, systemic infection of SnIV1 was likewise demonstrated using RT-PCR assays in different below- and above-ground parts of *S. villosum*, including roots, whole flowers, individual floral parts, and pollen. SnIV1 sequences were likewise found in a metatranscriptomic sequencing study of *Petunia* x *hybrida* (Solanaceae) flowers (Haselmair-Gosch et al. 2018). Collectively, such diverse source organisms or materials gave an unusual impression for a member of the *Ilarvirus* genus since its members are typically associated with a narrow range of natural hosts within one or a few families (Badillo-Vargas et al. 2016; Bratsch et al. 2019).

Moreover, SnIV1 was detected in the metatranscriptomic sequencing of insect samples from the USA and Belgium and, interestingly, in whole honeybees (*Apis mellifera*) (Deboutte et al. 2020), honeybee intestines (Tauber et al. 2022), and midgut (Vannette et al. 2015), as well as in abdomen of bumblebees (*Bombus impatiens*) (Costa et al. 2020). This information could imply the possibility of Apidae species harboring SnIV1 after alighting and feeding on SnIV1-infected plants or collecting SnIV1-infected pollen from them. Such a scenario has been reported for ilarviruses associated with bee species (Apidae) and thrips (mostly Thripidae) in several studies (Bristow and Martin 1999; Sharman et al. 2015; Roberts et al. 2018; Sdoodee and Teakle 1993). Furthermore, the detection of SnIV1 sequences in bees might suggest localization of SnIV1, not only in bee integumentary parts, but also in internal parts such as the gut, however, this needs further experimental verification. The detections of SnIV1 sequences in other sequenced animal tissues such as in *Daphnia magna* and human blood are suspicious and remain to be resolved, but it is very possible that these represent contaminations that occurred in the viromic experiments.

It is important to note that these findings from the viromic surveys and *in silico* search of SRA datasets do not necessarily imply that the sequenced materials are true hosts of SnlV1. Although mining of SRA datasets for viruses provided useful insights, verification of such sequence mining-derived information using another diagnostic method is mandatory but difficult (Lebas et al. 2022). Aside from true virus infection or symbiotic association with a certain organism, detection of viral sequence in an HTS dataset might result from wet lab contamination, index or barcode hopping, and cross-talk during sequencing (Lebas et al. 2022). It is likewise possible that other organisms that are the true hosts of SnIV1 could be present through an intimate (*e.g.* pathogen or symbiont) or casual association (*e.g.* as surface contaminant) with the primary sequenced sample. In such case, validation of HTS detection using a second diagnostic method and infectivity tests (if possible) are recommended (Kutnjak et al. 2021; Fox 2020).

On the possibility of pollen as vehicle for SnIV1 spread. Several ilarviruses and other members of family *Bromoviridae* were shown to be horizontally transmitted through pollen (Gilmer and Way 1960; George and Davidson 1963; Sdoodee and Teakle 1988; Greber et al. 1991; Mink 1993; Sdoodee and Teakle 1993; Aparicio et al. 1999; Card et al. 2007; Kawamura

et al. 2014; Jaspers et al. 2015). In some cases, ilarviruses were also reported to be associated with pollen surface or exine (Hamilton 1977; Digiaro and Savino 1992; Fetters et al. 2022). Pollen transmission, whether actively or passively with the aid of arthropod vectors (Mink 1993), and the pollen's inherent ubiquitous presence in the environment could result in erroneous assignation of natural host range of a virus, especially if sensitive diagnostic assays such as HTS or PCR are used. However, it is still an important horizontal transmission route that warrants special attention for emerging plant viruses. For instance, PMoV, the closest phylogenetically-related virus to SnIV1, was shown to be pollen-transmitted and thus poses threat for tomato production, at least in some European countries (Aramburu et al. 2010; Aparicio et al. 2018; Parrella et al. 2020).

Based on the results of this study, it is thus hypothesized that contamination by SnIV1-infected pollen might be one of the reasons (if not the most probable) for the identification of SnIV1 in different sequencing datasets. Detection of SnIV1 sequences in 39 datasets of leaf surface or epiphyte RNA sequencing from two Poaceae species (*Panicum* and *Miscanthus*) (Howe et al. 2023) fits well with such a hypothesis of surface contamination by pollen containing SnIV1. Thus, it is postulated that infected nearby crops or non-crop plants (most probably a Solanaceae species) could be a source of SnIV1-infected pollen that could make its way, passively or assisted by arthropod vectors, to neighboring plants. However, this hypothesis will need to be further investigated before it can be fully accepted.

Aside from plant species of the Fabaceae, Rosaceae, and Cannabaceae, SnIV1 was also associated with grapevines (infected with *Erysiphe necator* and *Plasmopara viticola*) in two viromic studies (Chiapello et al. 2020, 2019), and in additional two grapevine cultivars (Ugni Blanc and Sauvignon) from France that were sequenced in this study. Yet, cuttings from two French grapevines that had positive HTS and RT-PCR detections did not show evidence of SnlV1 presence when tested using RT-PCR several months after replanting as cuttings. This suggests either a localized or non-persistent infection in grapevine or, once again, that the first detection in field samples corresponds to surface contamination. Interestingly, another probable case of contamination is the detection of SnlV1 in *D. carota* subsp. *carota* (wild carrot). Out of 45 wild carrot populations (composite samples) (Schönegger 2023), only one showed SnlV1 reads, and this population happens to have been sampled close to the Sauvignon grapevines and SnlV1-infected *S. villosum* and *S. nigrum* plants at the INRAE Bordeaux research center.

Ilarvirus virions are known to be labile, but ilarviruses are also known to be pollen transmitted. This suggests that SnIV1 could potentially be efficiently protected and dispersed by pollen across distance and in various surfaces and source materials (Simkovich et al. 2021).

Patterns of variability and clustering of SnIV1 global isolates. Relatively low diversity was observed among isolates of SnIV1, across all genome segments, when compared to closely-related ilarviruses, such as TSV for which a comparable number of sequences was available. This result needs to be interpreted carefully, due to the possible uneven sampling (both by number and location) of the three compared viruses. Moreover, phylogenetic analyses showed only a partial clustering of SnIV1 isolates based on geographic origin with low ancestral

location probability when tested using a Bayesian framework. Although there is a distinct basal clade of isolates from European countries, no distinct pattern could be observed when the time of sampling (or sequencing) or broad category of possible hosts or source organism(s) (*i.e.*, plants or animals) were considered.

Host range and other modes of transmission of SnIV1. Two Solanaceae species were recently shown to be hosts of SnIV1, *C. annuum* (hybrid Arlequin F1) and *N. benthamiana* (Orfanidou et al. 2022). However, SnIV1 was not successfully mechanically transmitted to pepper plants in this study. This result might be explained by differences in inoculation procedures, inoculum source, or pepper genotypes used in the two studies. Furthermore, among eight plant species that were mechanically inoculated in the present study, infectivity of SnIV1 was demonstrated in three solanaceous species only: *N. occidentalis, S. nigrum,* and *N. benthamiana*. In a previous study (Ma et al. 2020), SnIV1 sequences were detected in both tomato and *S. nigrum* plants. However, in the present study, SnIV1 was successfully transmitted to *S. nigrum*, but not to the two tomatoes varieties (cv. Rudgers and M82). This suggests that association of SnIV1 with tomato in the Ma et al. (2020) study might be a result of surface contamination or, alternatively, differences in plant or virus genotype. Nevertheless, the infectivity of SnIV1 in a genotype of pepper raises the possibility that SnIV1 could be adapting to cultivated solanaceous hosts. It is worthwhile to note that both *S. villosum* and *S. nigrum* overwinter in at least some parts of Europe and may serve as reservoir of the virus during the winter months. Overwintering of SnIV1 is likely also possible through infected seeds, since vertical transmission through seeds of these two wild species was demonstrated here.

Summary and future perspectives. Overall, viromic surveys, extensive sequence database exploration, and literature searches conducted in this study resulted to the expansion of knowledge on the geographic distribution, possible hosts or source organisms, and diversity of SnlV1. In parallel, classical plant virology techniques facilitated the characterization of its pathobiology and possible modes of transmission. The properties of SnIV1 appear to be similar to those of other ilarviruses, but it is interestingly (and quite unexpectedly) associated much more frequently with very diverse plant samples and even with animal species mostly from Apidae. This raises further questions on unexplored properties of SnIV1 leading to its propensity to come up in unexpected HTS datasets. As discussed, many other ilarviruses are pollen-borne, including some infecting solanaceous species, although none have been reported in association with grapevines, despite the heavy HTS sequencing efforts performed in many laboratories around the world on this species. Although the present work facilitated progress in understanding aspects of the biology and epidemiology of SnIV1, there are still more information to be uncovered in order to fully understand this intriguing virus. Similar work could be implemented on other plant viruses poorly characterized but of similar biology and epidemiology in order to gain a certain level of preparedness for the possible global spread and disease outbreaks they may cause in the future.

Acknowledgments

The authors would like to thank the Sequencing Platform of Toulouse (GeT-PlaGe) for Illumina sequencing and for Marie Lefebvre for assisting in the processing of sequencing data. The authors are grateful for the assistance provided by Thierry Mauduit, Christophe Higelin and Maryam Khalili in the field, greenhouse, and sample preparation work. They are also grateful to Laure Beven for assisting in the use of dark field microscope, and Mickael Maucourt for assisting in tissue lyophilization. The authors would like to thank Varvara Maglioka and Reza M. Hajimorad for providing their SnIV1 genomic sequences ahead of release in GenBank and the publication of their papers.

Funding information

This work mainly received funding from Horizon 2020 Marie Skłodowska-Curie Actions Innovative Training Network (MSCA-ITN) project "Innovative Network for Next Generation Training and Sequencing of Virome (INEXTVIR)" (GA 813542) under the management of the European Commission-Research Executive Agency. It was also supported by the funding from Slovenian Research Agency (ARRS) financing (P4-0165, P4-0407, J4-4553). Funding for the work in Belgium was provided by The Belgian FPS Health Food Chain Safety and Environment under Project RT18/3 SEVIPLANT. MPS Rivarez also received funding from the *Balik* Scientist Program (Republic Act 11035) of the Department of Science and Technology – Philippine Council for Agriculture, Aquatic, and Natural Resources Research and Development (DOST–PCAARRD), Republic of the Philippines, during the manuscript writing and submission.

Author contributions

TC, AM, SM, MR, and DK are all involved in funding acquisition for the INEXTVIR project. TC, AM, MR, DK, and MPSR formulated and designed the study. TC supervised the study. MPSR did the majority of the experimental work, the data analyses, and wrote the first draft of the manuscript. TC contributed to sequence database mining and genome assembly. CF, AM and LSD contributed to collection and transmission experiments and RT-PCR testing of samples from France and assisted in greenhouse experiments. AP contributed in transmission experiments, nanopore sequencing and analyses, and in the transmission experiments. MTŽ did the light and transmission electron microscopy experiments. DS, SM, KDJ, and AB contributed SnIV1 sequences, and KDJ confirmed the detection of SnIV1 in Belgium by RT-PCR. DR helped in the conduct and interpretation of the phylogeographic analysis. All authors agreed and significantly contributed in editing the final manuscript.

Supporting Materials and Declarations

Details on Materials and Methods

Supplementary Figures and Tables

Supplementary Table 1. RT-PCR primer pairs used for the detection of SnIV1 and TBRV2.
Supplementary Table 2. Detection of SnIV1 from in silico searches of public sequence databases, sequence read archive datasets, and reports from literature.
Supplementary Figure 1. Percent pairwise identity among global SnIV1 isolates with their phylogenetic clustering.
Supplementary Figure 2. Ancestral reconstruction and discrete phylogeography of SnIV1 based on the Bayesian MCMC framework.

Data and analyses pipeline availability

Raw sequencing reads generated from this study were submitted in the NCBI Sequence Read Archive (SRA), collectively under with the BioProject accession number PRJNA874692, and in the Recherche Data Gouv platform (https://entrepot.recherche.data.gouv.fr/dataverse/inrae) with the persistent digital object identifier (doi): https://doi.org/10.57745/ZIXT4A. All SnIV1 genome sequences generated from this study were submitted to NCBI GenBank, and the accession numbers listed in Tables 1 and 3, and Supplementary Table 2. Details of the bioinformatic pipeline used for virus genome assembly is available through this link: https://gitlab.com/ilvo/phbn-wp2-training/-/tree/master/CLC_NIB_1.

Ethics declarations

The authors declare no competing interests.

LITERATURE CITED

Adams, M. J., and Antoniw, J. F. 2006. DPVweb: a comprehensive database of plant and fungal virus genes and genomes. Nucleic Acids Research. 34:D382–D385.

Adkins, S., Baker, C. A., Badillo-Vargas, I. E., Frantz, G., Mellinger, H. C., Roe, N., et al. 2015. Necrotic streak disease of tomato in Florida caused by a new ilarvirus species related to Tulare apple mosaic virus. New Disease Reports. 31:16.

Aparicio, F., Aramburu, J., Herranz, M. C., Pallás, V., and López, C. 2018. Parietaria mottle virus : a potential threat for tomato crops? Acta Horticulturae. 1207:261–268.

Aparicio, F., Sánchez-Pina, M. A., Sánchez-Navarro, J. A., and Pallás, V. 1999. Location of Prunus Necrotic Ringspot Ilarvirus Within Pollen Grains of Infected Nectarine Trees: Evidence from RT-PCR, Dot-blot and in situ Hybridisation. European Journal of Plant Pathology. 105:623–627.

Aramburu, J., Galipienso, L., Aparicio, F., Soler, S., and López, C. 2010. Mode of transmission of parietaria mottle virus. Journal of Plant Pathology. 92:679–684.

Arnoux, S. 2019. Comparative analyses of the molecular footprint of domestication in three Solanaceae species: eggplant, pepper and tomato (PhD Thesis). Available at: https://tel.archives-ouvertes.fr/tel-02185095v2/document.

Auber, R. P., Suttiyut, T., McCoy, R. M., Ghaste, M., Crook, J. W., Pendleton, A. L., et al. 2020. Hybrid de novo genome assembly of red gromwell (Lithospermum erythrorhizon) reveals evolutionary insight into shikonin biosynthesis. Horticulture Research. 7:82.

Badillo-Vargas, I. E., Baker, C. A., Turechek, W. W., Frantz, G., Mellinger, H. C., Funderburk, J. E., et al. 2016. Genomic and biological characterization of tomato necrotic streak virus, a novel subgroup 2 ilarvirus infecting tomato in Florida. Plant Disease. 100:1046–1053.

Bester, R., and Maree, H. J. 2023. First report of the plum marbling disease associated agent, plum viroid I, in apricots (Prunus armeniaca) in South Africa. Plant Disease. Available at: https://apsjournals.apsnet.org/doi/10.1094/PDIS-10-22-2321-PDN.

Bouckaert, R., Vaughan, T. G., Barido-Sottani, J., Duchêne, S., Fourment, M., Gavryushkina, A., et al. 2019. BEAST 2.5: An advanced software platform for Bayesian evolutionary analysis. PLoS Computational Biology. 15:e1006650.

Bratsch, S. A., Creswell, T. C., and Ruhl, G. E. 2018. First Report of Tomato Necrotic Spot Virus Infecting Tomato in Indiana. Plant Health Progress. 19:224–225.

Bratsch, S. A., Grinstead, S., Creswell, T. C., Ruhl, G. E., and Mollov, D. 2019. Characterization of Tomato Necrotic Spot Virus, a Subgroup 1 Ilarvirus Causing Necrotic Foliar, Stem, and Fruit Symptoms in Tomatoes in the United States. Plant Disease. 103:1391–1396.

Bristow, P. R., and Martin, R. R. 1999. Transmission and the Role of Honeybees in Field Spread of Blueberry Shock Ilarvirus, a Pollen-Borne Virus of Highbush Blueberry. Phytopathology®. 89:124–130.

Buzkan, N., Chiumenti, M., Massart, S., Sarpkaya, K., Karadağ, S., and Minafra, A. 2019. A new emaravirus discovered in Pistacia from Turkey. Virus Research. 263:159–163.

Card, S. D., Pearson, M. N., and Clover, G. R. G. 2007. Plant pathogens transmitted by pollen. Australasian Plant Pathology. 36:455–461.

Carroll, D., Daszak, P., Wolfe, N. D., Gao, G. F., Morel, C. M., Morzaria, S., et al. 2018. The Global Virome Project. Science. 359:872–874.

Chang, S., Puryear, J., and Cairney, J. 1993. A simple and efficient method for isolating RNA from pine trees. Plant Mol Biol Rep. 11:113–116.

Chen, X., Yang, Q., Li, H., Li, H., Hong, Y., Pan, L., et al. 2016. Transcriptome-wide sequencing provides insights into geocarpy in peanut (Arachis hypogaea L.). Plant Biotechnology Journal. 14:1215–1224.

Chiapello, M., Rodriguez-Romero, J., Ayllon, M., and Turina, M. 2019. A report on the virome of obligatory biotrophs. Available at: https://ec.europa.eu/research/participants/documents/downloadPublic?documentIds=080166e5c8e77dab&appId=PPGMS [Accessed February 7, 2022].

Chiapello, M., Rodríguez-Romero, J., Nerva, L., Forgia, M., Chitarra, W., Ayllón, M. A., et al. 2020. Putative new plant viruses associated with Plasmopara viticola -infected grapevine samples. Annals of Applied Biology. 176:180–191.

Coady, K. K., Burgoon, L., Doskey, C., and Davis, J. W. 2020. Assessment of Transcriptomic and Apical Responses of Daphnia magna Exposed to a Polyethylene Microplastic in a 21-d Chronic Study. Environmental Toxicology and Chemistry. 39:1578–1589.

Costa, C. P., Duennes, M. A., Fisher, K., Der, J. P., Watrous, K. M., Okamoto, N., et al. 2020. Transcriptome analysis reveals nutrition- and age-related patterns of gene expression in the fat body of pre-overwintering bumble bee queens. Molecular Ecology. 29:720–737.

Deboutte, W., Beller, L., Yinda, C. K., Maes, P., de Graaf, D. C., and Matthijnssens, J. 2020. Honey-bee–associated prokaryotic viral communities reveal wide viral diversity and a profound metabolic coding potential. Proceedings of the National Academy of Sciences. 117:10511–10519.

Dias, N. P., Hu, R., Hensley, D. D., Hansen, Z. R., Domier, L. L., and Hajimorad, M. R. 2022. A Survey for Viruses and Viroids of Peach in Tennessee Orchards by RNA Sequencing. Plant Health Progress. 23:265–268.

Digiaro, M., and Savino, V. 1992. Role of pollen and seeds in the spread of ilarviruses in almond. Advances in Horticultural Science. 6:134–136.

Edgar, R. C. 2004. MUSCLE: multiple sequence alignment with high accuracy and high throughput. Nucleic Acids Research. 32:1792–1797.

Edgar, R. C., Taylor, J., Lin, V., Altman, T., Barbera, P., Meleshko, D., et al. 2022. Petabase-scale sequence alignment catalyses viral discovery. Nature. 602:142–147.

Fetters, A. M., Cantalupo, P. G., Wei, N., Robles, M. T. S., Stanley, A., Stephens, J. D., et al. 2022. The pollen virome of wild plants and its association with variation in floral traits and land use. Nature Communications. 13:523.

Foissac, X., Svanella-Dumas, L., Gentit, P., Dulucq, M.-J., Marais, A., and Candresse, T. 2005. Polyvalent Degenerate Oligonucleotides Reverse Transcription-Polymerase Chain Reaction: A Polyvalent Detection and Characterization Tool for Trichoviruses, Capilloviruses, and Foveaviruses. Phytopathology®. 95:617–625.

Fontdevila, N., Khalili, M., Maachi, A., Rivarez, M. P. S., Rollin, R., Salavert, F., et al. 2023. Managing the deluge of newly discovered plant viruses and viroids: an optimized scientific and regulatory framework for their characterization and risk analysis. Frontiers in Microbiology. doi: 10.3389/fmicb.2023.1181562.

Fox, A. 2020. Reconsidering causal association in plant virology. Plant Pathology. 69:956–961.

Gaafar, Y. Z. A., Herz, K., Hartrick, J., Fletcher, J., Blouin, A. G., MacDiarmid, R., et al. 2020. Investigating the Pea Virome in Germany—Old Friends and New Players in the Field(s). Frontiers in Microbiology. 11:2605.

George, J. A., and Davidson, T. R. 1963. Pollen transmission of necrotic ring spot and sour cherry yellows viruses from tree to tree. Can. J. Plant Sci. 43:276–288.

Gilmer, R., and Way, R. 1960. Pollen transmission of necrotic ringspot and Prune dwarf viruses in Sour Cherry. Phytopathology. 50:624–625.

Greber, R. S., Klose, M. J., Milne, J. R., and Teakle, D. S. 1991. Transmission of prunus necrotic ringspot virus using plum pollen and thrips. Annals of Applied Biology. 118:589–593.

Gregory, A. C., Zayed, A. A., Conceição-Neto, N., Temperton, B., Bolduc, B., Alberti, A., et al. 2019. Marine DNA Viral Macro- and Microdiversity from Pole to Pole. Cell. 177:1109-1123.e14.

Hamilton, R. I. 1977. Surface Contamination of Pollen by Plant Viruses. Phytopathology®. 77:395.

Hammond, J., Adams, I., Fowkes, A. R., McGreig, S., Botermans, M., van Oorspronk, J. J. A., et al. 2020. Sequence analysis of 43-year old samples of Plantago lanceolata show that Plantain virus X is synonymous with Actinidia virus X and is widely distributed. Plant Pathology. 70:249–258.

Haselmair-Gosch, C., Miosic, S., Nitarska, D., Roth, B. L., Walliser, B., Paltram, R., et al. 2018. Great Cause—Small Effect: Undeclared Genetically Engineered Orange Petunias Harbor an Inefficient Dihydroflavonol 4-Reductase. Frontiers in Plant Science. 9:149.

Hou, W., Li, S., and Massart, S. 2020. Is There a "Biological Desert" With the Discovery of New Plant Viruses? A Retrospective Analysis for New Fruit Tree Viruses. Frontiers in Microbiology. 11:592816.

Hou, X., He, Y., Fang, P., Mei, S.-Q., Xu, Z., Wu, W.-C., et al. 2023. Artificial intelligence redefines RNA virus discovery. :2023.04.18.537342 Available at: https://www.biorxiv.org/content/10.1101/2023.04.18.537342v1 [Accessed April 19, 2023].

Howe, A., Stopnisek, N., Dooley, S. K., Yang, F., Grady, K. L., and Shade, A. 2023. Seasonal activities of the phyllosphere microbiome of perennial crops. Nature Communications. 14:1039.

ICTV. 2023. Current ICTV Taxonomy Release. Available at: https://ictv.global/taxonomy [Accessed April 10, 2023].

Jaspers, M. V., Falloon, P. G., and Pearson, M. N. 2015. Seed and pollen transmission of asparagus virus 2. European Journal of Plant Pathology. 142:173–183.

Kawamura, R., Shimura, H., Mochizuki, T., Ohki, S. T., and Masuta, C. 2014. Pollen Transmission of Asparagus virus 2 (AV-2) May Facilitate Mixed Infection by Two AV-2 Isolates in Asparagus Plants. Phytopathology®. 104:1001–1006.

Khalili, M., Candresse, T., Koloniuk, I., Safarova, D., Brans, Y., Faure, C., et al. 2023. The expanding menagerie of Prunus-infecting luteoviruses. Phytopathology®. 113:345–354.

Kibbe, W. A. 2007. OligoCalc: an online oligonucleotide properties calculator. Nucleic Acids Research. 35:W43–W46.

de Klerk, A., Swanepoel, P., Lourens, R., Zondo, M., Abodunran, I., Lytras, S., et al. 2022. Conserved recombination patterns across coronavirus subgenera. Virus Evolution. 8:1–15.

Kumar, S., Kumar, G. S., Maitra, S. S., Malý, P., Bharadwaj, S., Sharma, P., et al. 2022. Viral informatics: bioinformatics-based solution for managing viral infections. Briefings in Bioinformatics. 23:1–36.

Kumar, S., Stecher, G., Li, M., Knyaz, C., and Tamura, K. 2018. MEGA X: Molecular Evolutionary Genetics Analysis across Computing Platforms. Molecular Biology and Evolution. 35:1547–1549.

Kutnjak, D., Tamisier, L., Adams, I., Boonham, N., Candresse, T., Chiumenti, M., et al. 2021. A Primer on the Analysis of High-Throughput Sequencing Data for Detection of Plant Viruses. Microorganisms. 9:841.

Lauber, C., and Seitz, S. 2022. Opportunities and Challenges of Data-Driven Virus Discovery. Biomolecules. 12:1073.

Lebas, B., Adams, I., Al Rwahnih, M., Baeyen, S., Bilodeau, G. J., Blouin, A. G., et al. 2022. Facilitating the adoption of high-throughput sequencing technologies as a plant pest diagnostic test in laboratories: A step-by-step description. EPPO Bulletin. 52:394–418.

Ledón-Rettig, C. C., Zattara, E. E., and Moczek, A. P. 2017. Asymmetric interactions between doublesex and tissue- and sex-specific target genes mediate sexual dimorphism in beetles. Nature Communications. 8:14593.

Lee, B. D., Neri, U., Roux, S., Wolf, Y. I., Camargo, A. P., Krupovic, M., et al. 2023. Mining metatranscriptomes reveals a vast world of viroid-like circular RNAs. Cell. 186:P646-661.E4.

Letunic, I., and Bork, P. 2021. Interactive Tree Of Life (iTOL) v5: an online tool for phylogenetic tree display and annotation. Nucleic Acids Research. 49:W293–W296.

Ma, Y., Marais, A., Lefebvre, M., Faure, C., and Candresse, T. 2020. Metagenomic analysis of virome cross-talk between cultivated Solanum lycopersicum and wild Solanum nigrum. Virology. 540:38–44.

Ma, Y., Marais, A., Lefebvre, M., Theil, S., Svanella-Dumas, L., Faure, C., et al. 2019. Phytovirome Analysis of Wild Plant Populations: Comparison of Double-Stranded RNA and Virion-Associated Nucleic Acid Metagenomic Approaches. Journal of Virology. 94:e01462-19.

Maclot, F., Candresse, T., Filloux, D., Malmstrom, C. M., Roumagnac, P., van der Vlugt, R., et al. 2020. Illuminating an ecological blackbox: using high throughput sequencing to characterize the plant virome across scales. Frontiers in Microbiology. 11:578064.

Mahlanza, T., Pierneef, R. E., Makwarela, L., Roberts, R., and van der Merwe, M. 2022. Metagenomic analysis for detection and discovery of plant viruses in wild Solanum spp. in South Africa. Plant Pathology. 71:1633–1644.

Marais, A., Faure, C., Couture, C., Bergey, B., Gentit, P., and Candresse, T. 2014. Characterization by Deep Sequencing of Divergent Plum bark necrosis stem pitting-associated virus (PBNSPaV) Isolates and Development of a Broad-Spectrum PBNSPaV Detection Assay. Phytopathology®. 104:660–666.

Martin, D. P., Varsani, A., Roumagnac, P., Botha, G., Maslamoney, S., Schwab, T., et al. 2021. RDP5: a computer program for analyzing recombination in, and removing signals of recombination from, nucleotide sequence datasets. Virus Evolution. 7:veaa087.

Massart, S., Candresse, T., Gil, J., Lacomme, C., Predajna, L., Ravnikar, M., et al. 2017. A framework for the evaluation of biosecurity, commercial, regulatory, and scientific impacts of plant viruses and viroids identified by NGS technologies. Frontiers in Microbiology. 8:45.

McLeish, M. J., Fraile, A., and García-Arenal, F. 2021. Population Genomics of Plant Viruses: The Ecology and Evolution of Virus Emergence. Phytopathology®. 111:32–39.

Meurens, F., Dunoyer, C., Fourichon, C., Gerdts, V., Haddad, N., Kortekaas, J., et al. 2021. Animal board invited review: Risks of zoonotic disease emergence at the interface of wildlife and livestock systems. Animal. 15:100241.

Mifsud, J. C. O., Gallagher, R. V., Holmes, E. C., and Geoghegan, J. L. 2022. Transcriptome Mining Expands Knowledge of RNA Viruses across the Plant Kingdom. Journal of Virology. 96:e00260-22.

Mink, G. I. 1993. Pollen and Seed-Transmitted Viruses and Viroids. Annual Review of Phytopathology. 31:375–402.
Morens, D. M., Daszak, P., Markel, H., and Taubenberger, J. K. 2020. Pandemic COVID-19 Joins History's Pandemic Legion. mBio. 11:e00812-20.
Muhire, B. M., Varsani, A., and Martin, D. P. 2014. SDT: A Virus Classification Tool Based on Pairwise Sequence Alignment and Identity Calculation ed. Jens H. Kuhn. PLoS ONE. 9:e108277.
Natsume, S., Takagi, H., Shiraishi, A., Murata, J., Toyonaga, H., Patzak, J., et al. 2015. The Draft Genome of Hop (Humulus lupulus), an Essence for Brewing. Plant and Cell Physiology. 56:428–441.
Neri, U., Wolf, Y. I., Roux, S., Camargo, A. P., Lee, B., Kazlauskas, D., et al. 2022. Expansion of the global RNA virome reveals diverse clades of bacteriophages. Cell. 185:4023–4037.
Orfanidou, C. G., Katiou, D., Papadopoulou, E., Katis, N. I., and Maliogka, V. I. 2022. A known ilarvirus is associated with a novel viral disease in pepper. Plant Pathology. 71:1901–1909.
Palanga, E., Filloux, D., Martin, D. P., Fernandez, E., Gargani, D., Ferdinand, R., et al. 2016. Metagenomic-Based Screening and Molecular Characterization of Cowpea-Infecting Viruses in Burkina Faso. PLOS ONE. 11:e0165188.
Pallas, V., Aparicio, F., Herranz, M. C., Amari, K., Sanchez-Pina, M. A., Myrta, A., et al. 2012. Ilarviruses of Prunus spp.: A Continued Concern for Fruit Trees. Phytopathology®. 102:1108–1120.
Parrella, G., Troiano, E., Cherchi, C., and Giordano, P. 2020. Severe outbreaks of Parietaria mottle virus in tomato in Sardinia, southern Italy. Journal of Plant Pathology. 102:915–915.
Pecman, A., Adams, I., Gutiérrez-Aguirre, I., Fox, A., Boonham, N., Ravnikar, M., et al. 2022. Systematic Comparison of Nanopore and Illumina Sequencing for the Detection of Plant Viruses and Viroids Using Total RNA Sequencing Approach. Frontiers in Microbiology. 13:1424.
Pecman, A., Kutnjak, D., Gutiérrez-Aguirre, I., Adams, I., Fox, A., Boonham, N., et al. 2017. Next Generation Sequencing for Detection and Discovery of Plant Viruses and Viroids: Comparison of Two Approaches. Frontiers in Microbiology. 8:1–10.
Poudel, B., Ho, T., Laney, A., Khadgi, A., and Tzanetakis, I. E. 2014. Epidemiology of Blackberry chlorotic ringspot virus. Plant Disease. 98:547–550.
Rai, A., Nakaya, T., Shimizu, Y., Rai, M., Nakamura, M., Suzuki, H., et al. 2018. De Novo Transcriptome Assembly and Characterization of Lithospermum officinale to Discover Putative Genes Involved in Specialized Metabolites Biosynthesis. Planta Medica. 84:920–934.
Ristaino, J. B., Anderson, P. K., Bebber, D. P., Brauman, K. A., Cunniffe, N. J., Fedoroff, N. V., et al. 2021. The persistent threat of emerging plant disease pandemics to global food security. Proceedings of the National Academy of Sciences. 118:e2022239118.
Rivarez, M. P. S., Pecman, A., Bačnik, K., Maksimović, O., Vučurović, A., Seljak, G., et al. 2023. In-depth study of tomato and weed viromes reveals undiscovered plant virus diversity in an agroecosystem. Microbiome. 11:60.
Rivarez, M. P. S., Vučurović, A., Mehle, N., Ravnikar, M., and Kutnjak, D. 2021. Global Advances in Tomato Virome Research: Current Status and the Impact of High-Throughput Sequencing. Frontiers in Microbiology. 12:671925.
Roberts, J. M. K., Ireland, K. B., Tay, W. T., and Paini, D. 2018. Honey bee-assisted surveillance for early plant virus detection. Annals of Applied Biology. 173:285–293.

Roux, B., Rodde, N., Jardinaud, M.-F., Timmers, T., Sauviac, L., Cottret, L., et al. 2014. An integrated analysis of plant and bacterial gene expression in symbiotic root nodules using laser-capture microdissection coupled to RNA sequencing. The Plant Journal. 77:817–837.

Rozas, J., Ferrer-Mata, A., Sánchez-DelBarrio, J. C., Guirao-Rico, S., Librado, P., Ramos-Onsins, S. E., et al. 2017. DnaSP 6: DNA Sequence Polymorphism Analysis of Large Data Sets. Molecular Biology and Evolution. 34:3299–3302.

Schönegger, D. 2023. Analysis of the virome and reciprocal transfers of viruses between cultivated and wild carrot populations (PhD Thesis). Available at: https://theses.hal.science/tel-04033935.

Sdoodee, R., and Teakle, D. 1988. Seed and pollen transmission of tobacco streak virus in tomato (Lycopersicon esculentum cv. Grosse Lisse). Australian Journal of Agricultural Research. 39:469.

Sdoodee, R., and Teakle, D. S. 1993. Studies on the mechanism of transmission of pollen-associated tobacco streak ilarvirus virus by Thrips tabaci. Plant Pathology. 42:88–92.

Sharman, M. 2015. Epidemiology and genetic diversity of Tobacco streak virus and related subgroup 1 ilarviruses (BSc Thesis). Available at: http://espace.library.uq.edu.au/view/UQ:372151.

Sharman, M., Thomas, J. e., and Persley, D. m. 2015. Natural host range, thrips and seed transmission of distinct Tobacco streak virus strains in Queensland, Australia. Annals of Applied Biology. 167:197–207.

Simkovich, A., Kohalmi, S. E., and Wang, A. 2021. Ilarviruses (Bromoviridae). In *Encyclopedia of Virology (Fourth Edition)*, eds. Dennis H. Bamford and Mark Zuckerman. Oxford: Academic Press, p. 439–446.

Sproviero, D., Gagliardi, S., Zucca, S., Arigoni, M., Giannini, M., Garofalo, M., et al. 2021. Different miRNA Profiles in Plasma Derived Small and Large Extracellular Vesicles from Patients with Neurodegenerative Diseases. International Journal of Molecular Sciences. 22:2737.

Stewart, C., Kon, T., Rojas, M., Graham, A., Martin, D., Gilbertson, R., et al. 2014. The molecular characterisation of a Sida-infecting begomovirus from Jamaica. Arch Virol. 159:375–378.

Subramanian, S. 2016. The effects of sample size on population genomic analyses – implications for the tests of neutrality. BMC Genomics. 17:123.

Svanella-Dumas, L., Candresse, T., Lefebvre, M., Lluch, J., Valiere, S., Larignon, P., et al. 2022. First Report of Grapevine Virus L Infecting Grapevine in Southeast France. Plant Disease. 106:1536.

Tauber, J. P., McMahon, D., Ryabov, E. V., Kunat, M., Ptaszyńska, A. A., and Evans, J. D. 2022. Honeybee intestines retain low yeast titers, but no bacterial mutualists, at emergence. Yeast. 39:95–107.

Temple, C., Blouin, A. G., Boezen, D., Botermans, M., Durant, L., Jonghe, K. D., et al. 2023. Biological characterization of an emergent virus infecting vegetables in diversified production systems: physostegia chlorotic mottle virus. Available at: https://www.biorxiv.org/content/10.1101/2023.04.03.535357v2.

Temple, C., Blouin, A. G., De Jonghe, K., Foucart, Y., Botermans, M., Westenberg, M., et al. 2022. Biological and Genetic Characterization of Physostegia Chlorotic Mottle Virus in Europe Based on Host Range, Location, and Time. Plant Disease. 106:2797–2807.

Vannette, R. L., Mohamed, A., and Johnson, B. R. 2015. Forager bees (Apis mellifera) highly express immune and detoxification genes in tissues associated with nectar processing. Scientific Reports. 5:16224.

Vargas-Asencio, J., McLane, H., Bush, E., and Perry, K. L. 2013. Spinach latent virus Infecting Tomato in Virginia, United States. Plant Disease. 97:1663.

Verhoeven, A., Kloth, K. J., Kupczok, A., Oymans, G. H., Damen, J., Rijnsburger, K., et al. 2023. Arabidopsis latent virus 1, a comovirus widely spread in Arabidopsis thaliana collections. New Phytologist. 237:1146–1153.

Wu, M., Kostyun, J. L., Hahn, M. W., and Moyle, L. C. 2018. Dissecting the basis of novel trait evolution in a radiation with widespread phylogenetic discordance. Molecular Ecology. 27:3301–3316.

Xu, C., Sun, X., Taylor, A., Jiao, C., Xu, Y., Cai, X., et al. 2017. Diversity, Distribution, and Evolution of Tomato Viruses in China Uncovered by Small RNA Sequencing. Journal of Virology. 91:e00173-17.

Zayed, A. A., Wainaina, J. M., Dominguez-Huerta, G., Pelletier, E., Guo, J., Mohssen, M., et al. 2022. Cryptic and abundant marine viruses at the evolutionary origins of Earth's RNA virome. Science. 376:156–162.

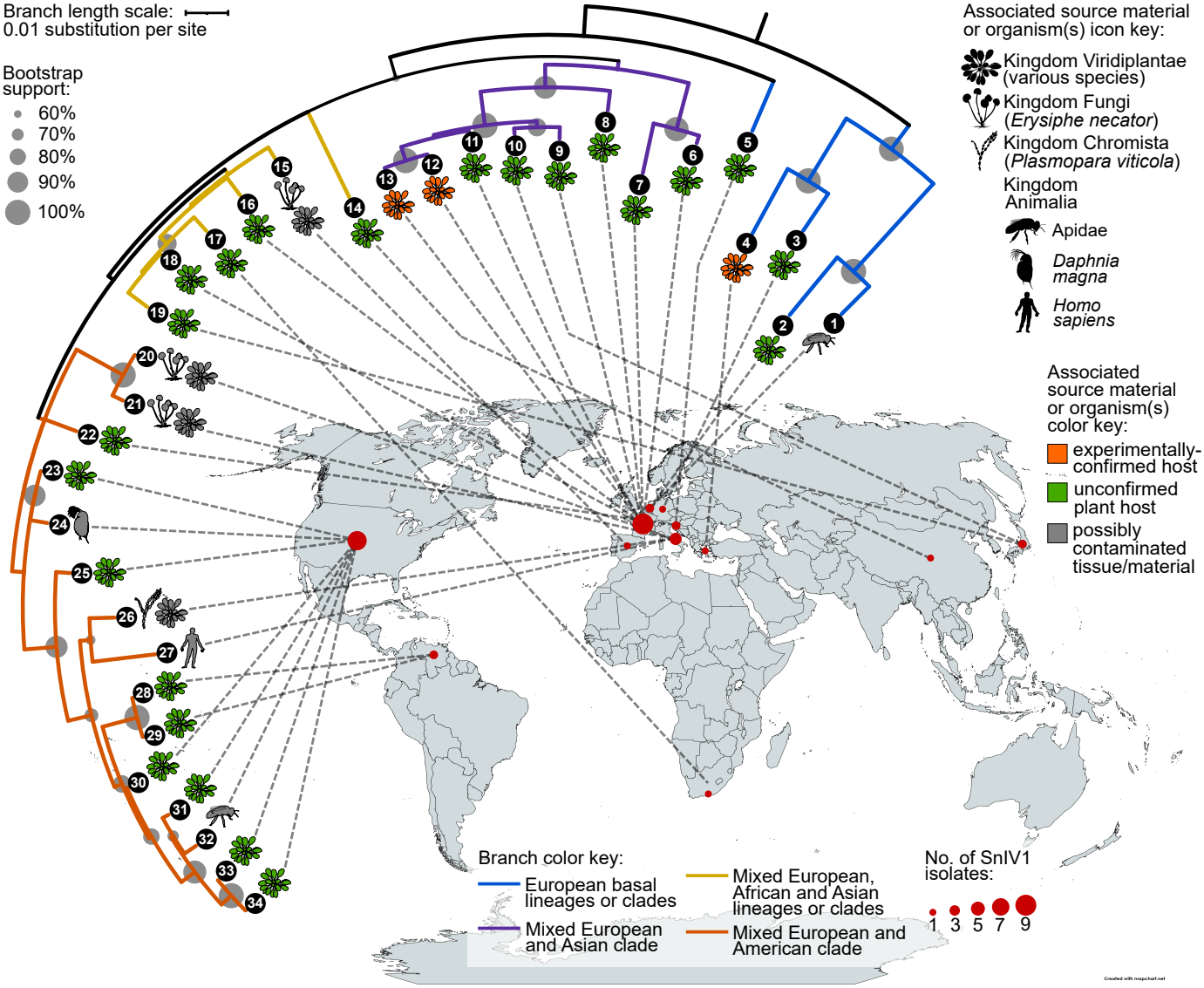
Branch length scale:
0.01 substitution per site
Bootstrap support:
60%
70%
80%
90%
100%
Associated source material or organism(s) icon key:
Kingdom Viridiplantae (various species)
Kingdom Fungi (Erysiphe necator)
Kingdom Chromista (Plasmopara viticola)
Kingdom Animalia
Apidae
Daphnia magna
Homo sapiens
Associated source material or organism(s) color key:
experimentally-confirmed host
unconfirmed plant host
possibly contaminated tissue/material
Branch color key:
European basal lineages or clades
Mixed European and Asian clade
Mixed European, African and Asian lineages or clades
Mixed European and American clade
No. of SnIV1 isolates:
1 3 5 7 9

Figure 1

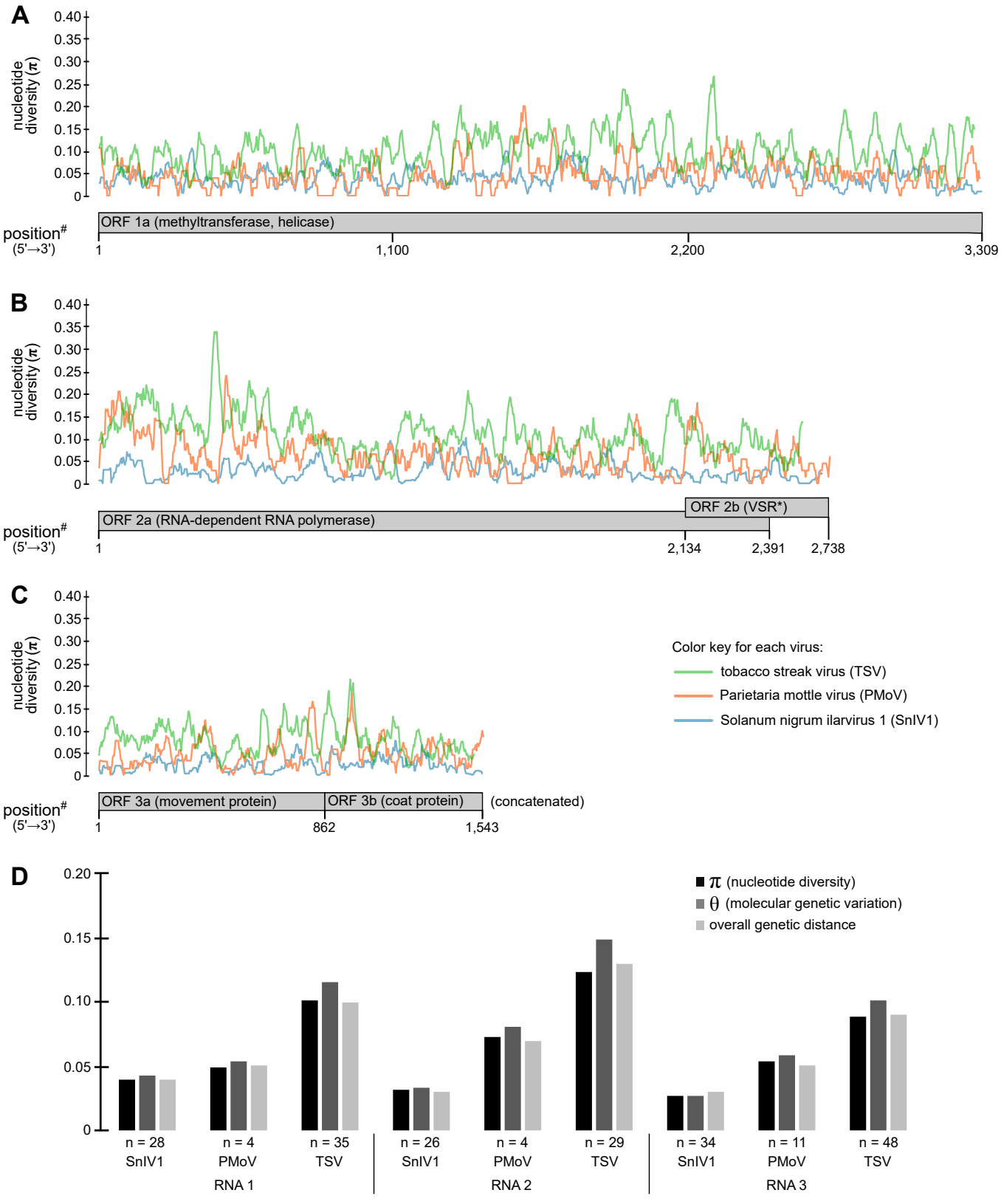
A
nucleotide diversity (π)
0.40
0.35
0.30
0.25
0.20
0.15
0.10
0.05
0
position#
(5'→3')
ORF 1a (methyltransferase, helicase)
1
1,100
2,200
3,309
B
nucleotide diversity (π)
position#
(5'→3')
ORF 2a (RNA-dependent RNA polymerase)
ORF 2b (VSR*)
1
2,134
2,391
2,738
C
nucleotide diversity (π)
position#
(5'→3')
ORF 3a (movement protein)
ORF 3b (coat protein)
(concatenated)
1
862
1,543
Color key for each virus:
tobacco streak virus (TSV)
Parietaria mottle virus (PMoV)
Solanum nigrum ilarvirus 1 (SnIV1)
D
0.20
0.15
0.10
0.05
0
π (nucleotide diversity)
θ (molecular genetic variation)
overall genetic distance
n = 28
SnIV1
n = 4
PMoV
n = 35
TSV
RNA 1
n = 26
SnIV1
n = 4
PMoV
n = 29
TSV
RNA 2
n = 34
SnIV1
n = 11
PMoV
n = 48
TSV
RNA 3

Figure 2

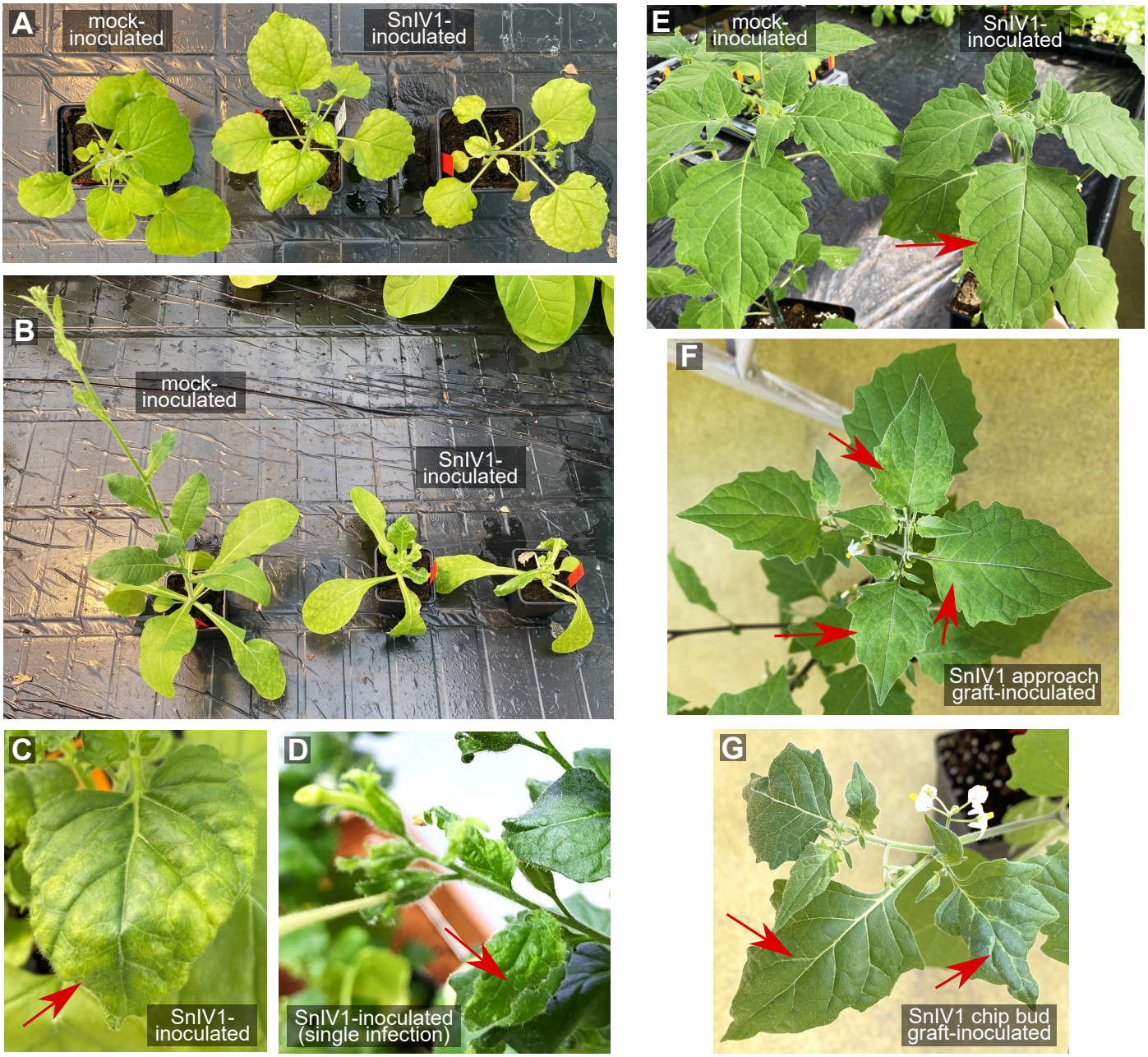
A
mock-inoculated
SnIV1-inoculated
B
mock-inoculated
SnIV1-inoculated
C
SnIV1-inoculated
D
SnIV1-inoculated (single infection)
E
mock-inoculated
SnIV1-inoculated
F
SnIV1 approach graft-inoculated
G
SnIV1 chip bud graft-inoculated

Figure 3

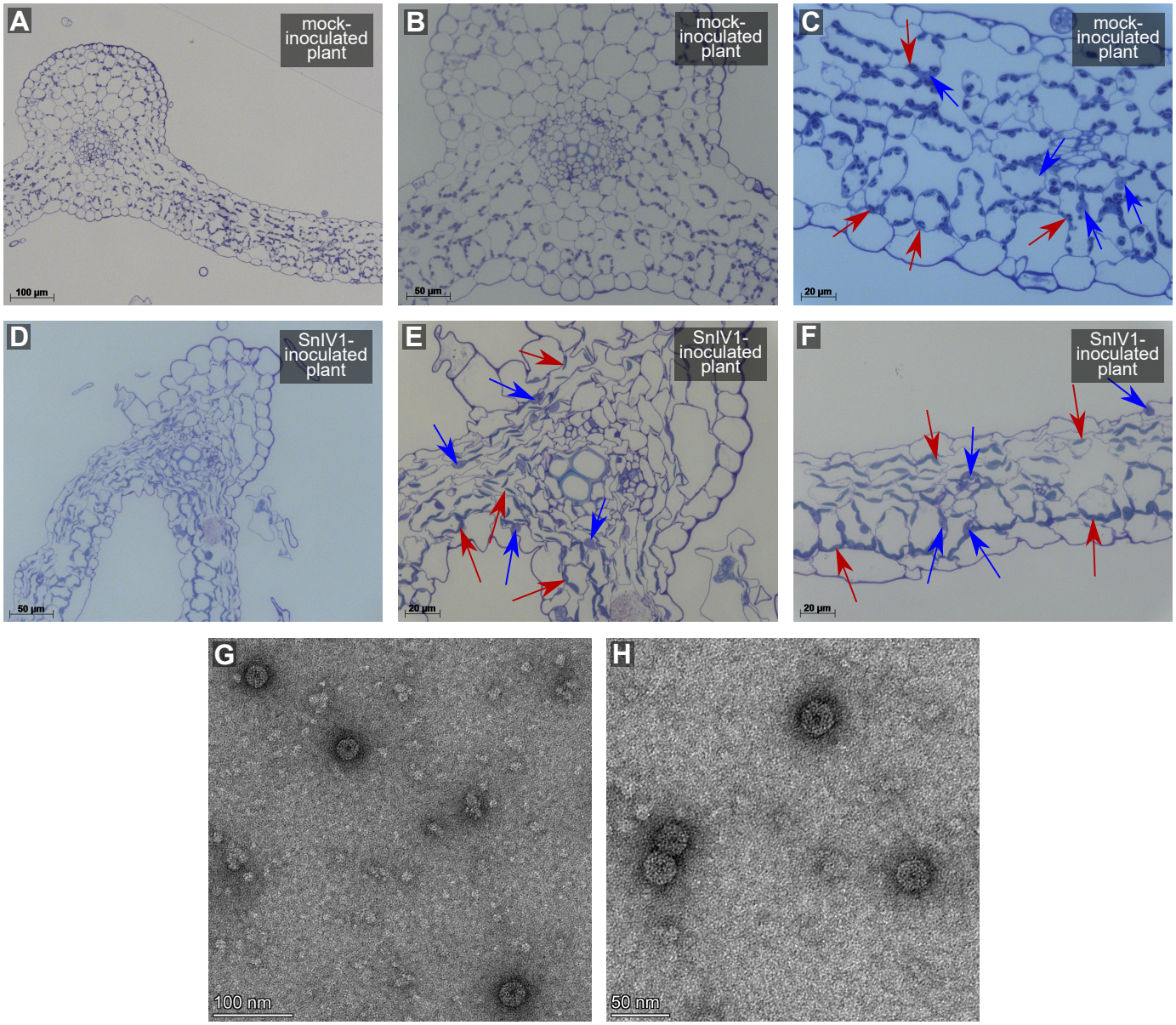
A
mock-inoculated plant
100 µm
B
mock-inoculated plant
50 µm
C
mock-inoculated plant
20 µm
D
SnIV1-inoculated plant
50 µm
E
SnIV1-inoculated plant
20 µm
F
SnIV1-inoculated plant
20 µm
G
100 nm
H
50 nm

Figure 4

Diversity and pathobiology of an ilarvirus unexpectedly detected in diverse plants and global sequencing data

Mark Paul Selda Rivarez,[1,†,*] Chantal Faure,[2] Laurence Svanella-Dumas,[2] Anja Pecman,[1] Magda Tušek-Žnidaric,[1] Deborah Schönegger,[2] Kris De Jonghe,[3] Arnaud Blouin,[4,‡], David A. Rasmussen[5,6], Sebastien Massart,[4] Maja Ravnikar,[1] Denis Kutnjak,[1] Armelle Marais,[2] and Thierry Candresse[2,*]

[1]Department of Biotechnology and Systems Biology, National Institute of Biology, Ljubljana, 1000, Slovenia
[2]Univ. Bordeaux, INRAE, UMR 1332 Biologie du Fruit et Pathologie, Villenave d'Ornon, 33882, France
[3]Plant Sciences Unit, Flanders Research Institute for Agriculture, Fisheries and Food, Merelbeke, 9820, Belgium
[4]Plant Pathology Laboratory, TERRA-Gembloux Agro-Bio Tech, University of Liège, Gembloux, 5030, Belgium
[†]present affiliations: [5]Department of Entomology and Plant Pathology, North Carolina State University, Raleigh, 27606, USA; [6]Bioinformatics Research Center, North Carolina State University, 27607, USA; College of Agriculture and Agri-Industries, Caraga State University, Butuan City, 8600, Philippines
[‡]present affiliation: Plant Protection Department, Agroscope, Nyon, 1260, Switzerland
*corresponding authors: M.P.S. Rivarez (mpsrivarez@gmail.com) and T. Candresse (thierry.candresse@inrae.fr)

Details on Materials and Methods

Nanopore sequencing. A CTAB-based protocol (Chang et al. 1993) was used to extract total RNAs from SnIV1-infected *S. villosum* that served as inoculum and from inoculated *N. benthamiana* prior to Nanopore sequencing. Total RNAs extracted were then treated with DNase using the TURBO DNA-free™ Kit (Thermo Fisher Scientific, USA). RNA quality and quantity were checked prior to sequencing using an Epoch™ microplate spectrophotometer (BioTek, Agilent, USA) and a QuBit fluorometer (Thermo Fisher Scientific, USA). Nanopore sequencing was performed as previously described (Rivarez et al. 2023; Pecman et al. 2022). Briefly, total RNAs were depleted of ribosomal RNA using the RiboMinus™ Plant Kit (Thermo Fisher Scientific, USA) and polyadenylated using *E. coli* Poly(A) polymerase (New England Biolabs, UK). cDNA libraries were prepared using the PCR-cDNA barcoding kit (catalog no. SQK-PCB109, version 10Oct2019, Oxford Nanopore Technologies (ONT), UK), and sequencing was performed using the ONT MinION platform (ONT, UK) with base-calling following a previously described workflow (Pecman et al. 2022).

Search for SnIV1 sequences in databases and the literature and assembly of SnIV1 genomes. Publicly available databases and the literature were searched for SnIV1 sequences to obtain additional SnIV1 genomes. Firstly, NCBI GenBank database release version (r.v.) 250

that includes nucleotide, whole genome shotgun (WGS), transcriptome shotgun assembly (TSA) sequences, *etc*. (Sayers et al. 2022) was searched using the BLASTn algorithm (Altschul et al. 1997), with SnIV1 genomic segments (GenBank accession number (a.n.) OL472060-OL472062) as queries. The search was performed on July 22, 2022. Percent identity and percent query coverage values were both set at greater than 90% as threshold to select significant BLASTn hits.

Secondly, a search in global metagenomes, metatranscriptomes, or metaviromes was performed through a palmID search in Serratus (https://serratus.io/palmid) (Edgar et al. 2022), which analyzed and annotated in a database (palmDB) around 5.7 million global SRA datasets deposited as of January 2021. The SnIV1 RNA 2 sequence (a.n. OL472061) which contains the RNA-dependent RNA polymerase (RdRp) domain needed for the palmID search was used as query. A 100% RdRp 'palmprint' (Babaian and Edgar 2022) amino acid identity and an E-value less than $8.4x10^{-74}$ were used as thresholds to identify significant palmID hits since it was the lowest E-value given by the palmID search for 100% identity hits.

Third, published literature was searched using Google Scholar (https://scholar.google.com/) with the queries 'Solanum nigrum ilarvirus 1', 'grapevine-associated ilarvirus', or 'surrounding legume-associated ilarvirus', which are the first three virus names proposed for SnIV1. The search was performed on August 3, 2022. SnIV1 sequences that were not yet available in GenBank r.v. 250 were requested from the authors of the studies that identified the virus prior to their release in NCBI or as official publication.

A previously described bioinformatic pipeline was used for the reference-guided assembly of SnIV1 genomes from HTS data in this study (Pecman et al. 2017; Rivarez et al. 2023). Using the pipeline that was run in CLC Genomics Workbench (GWB) version (v.) 20 (Qiagen, USA), barcodes were removed from raw reads that were previously screened based on phred quality scores. Virus and virus-like reads and contigs were initially identified by mapping reads and contigs to the virus RefSeq database r.v. 212 (Sayers et al. 2022) and by viral domain searches in contigs against the pFam v. 33 (Mistry et al. 2021). SnIV1 consensus genomes were reconstructed by mapping reads to the genome of a Slovenian isolate (a.n. OL472060-OL472062), with percent identity and genome coverage threshold set at ≥90%. Mapping profiles were visually inspected in CLC-GWB and mean read depth (mrd), also known as average coverage, or on average, the number of times each locus in a reference genome is covered by mapped reads was noted. mrd is calculated by getting the sum of all mapped read depths at each locus and dividing it by the number of bases or the length of the reference (Illumina 2023). The number of mapped reads, percent genome covered, and the presence of a complete set of open reading frames (ORFs) were noted, in reference to some recommendations for the detection of virus genomes in metagenomic data (Roux et al. 2019; Simmonds et al. 2017). Genomes assembled from SRA datasets were deposited in GenBank as third party annotations.

In parallel efforts, a previously described method was used to *de novo* assemble and annotate contigs from HTS data obtained from Belgian samples (Buzkan et al. 2019). When needed, contigs representing SnIV1 genome segments were extended by iterative mapping of reads as implemented in Geneious Prime v. 2022.1.1 (Dotmatics, USA).

A customized workflow (Pecman et al. 2022) was used to assemble SnIV1 genomes from ONT MinION sequencing data of *S. villosum* (inoculum) and inoculated *N. benthamiana*. The workflow was used for quality screening, barcode trimming, demultiplexing, visualization, and *de novo* assembly. Minimap2 v. 2.24 (Li 2018) as implemented in Geneious Prime v. 2022.1.1 (Dotmatics, USA) was used for mapping reads or contigs to viral RefSeq r.v. 212 (Sayers et al. 2022) and SnIV1 genome (a.n. OL472060-OL472062).

Bayesian phylogeographic analysis in BEAST. We performed a Bayesian phylogeographic analysis in BEAST v. 2.7.4 based on the procedure presented in http://beast2-dev.github.io/beast-docs/beast2/PhylogeographyDiscrete/AR.html, with concepts described in (Bouckaert et al. 2019). Convergence of values of parameters from the BEAST analysis such as 'posterior', 'likelihood', and 'posterior', among others, when examined in a trace graph using Tracer v. 1.7.2, included in the BEAST v. 2.7.4 package. The final tree was annotated using FigTree v. 1.4.4, included in the BEAST v. 2.7.4 package.

Supplementary Table 1. RT-PCR primer pairs used for the detection of SnIV1 and TBRV2.

Source	Target	Sequence	Annealing Temp. (˚C)	Amplicon size (bp)
this study	SnIV1 RNA1	Forward: 5'-AGTTGAGATGACTCTGAGTATG-3' Reverse: 5'-TCAATCCAGGGGAAATCATCTT-3'	56	284
	SnIV1 RNA3	Forward: 5'-GATGTTGAAATGTTTGGCTA-3' Reverse: 5'-GCATACGTCTCCAGGGCTCT-3'	56	285
	SnIV1 RNA3	Forward: 5'-GCTTCTTGGACTTACCTGGAATG-3' Reverse: 5'-AAACGCCATTGACCACGCCATAG-3'	60	499
(Rivarez et al. 2023)	SnIV1 RNA3	Forward: 5'-GTATGAAAACTTCAACCTCTCC-3' Reverse: 5'-ATATAGCTACCCAGAAATCAGC-3'	52	669
	TBRV2	Forward: 5'-TTCCTGTTCATTATCACAATGC-3' Reverse: 5'-GTTAGTTGACCAAGAGTACCAG-3'	51	596

Supplementary Table 2. Detection of SnIV1 from *in silico* searches of public sequence databases, sequence read archive datasets, and reports from literature. All BLASTn hits are >90% identical to SnIV1 sequences (a.n. OL472060-OL472062) (E-value < 10^{-4}), while Serratus-palmID hits are 100% identical to SnIV1 RdRp palmprint (E-value < 10^{-74}).

Method of search	Associated literature and geographic origin	Biological sample(s) sequenced[a]			NCBI accession number (SRA / GenBank)[b]
		Classification	Scientific name	Tissue	
BLASTn GenBank search	(Rivarez et al. 2023); Slovenia	Viridiplantae / Solanaceae	*Physalis* sp.*	leaf	SRR16552283 / OL472060-OL472062[c,(5)]
		Viridiplantae	unidentified weed species	leaf	SRR16552232 / OP561313-OP561315[(22)]
	(Gaafar et al. 2020); Germany	Viridiplantae / Fabaceae	unidentified weed species	leaf	MN412725-MN412727[d,(3)]
	(Ma et al. 2020); France	Viridiplantae / Solanaceae	*Solanum nigrum**	leaf	sequence dataset available at doi.org/10.15454/S486RR / MN216375, MN216370, MN216373, MN216376[(11)]
			Solanum lycopersicum	leaf	MN216371, MN216374, MN216377[(16)], MN216372, MN216378
	(Chiapello et al. 2020)[e], Italy	Viridiplantae / Vitaceae	*Vitis vinifera* (*Plasmopara viticola*-infected)	leaf	SRR11364881, SRR11364883-SRR11364887, SRR11364893, SRR9995125, SRR9995127-SRR9995131 / MN520742-MN520744[(26)]
	(Chiapello et al. 2019)[f]; Spain	Viridiplantae / Vitaceae	*V. vinifera* (*Erysiphe necator*-infected)	leaf	MN630191, MN630189, MN630188[(15)]
	(Natsume et al. 2015); Japan	Viridiplantae / Cannabaceae	*Humulus lupulus* var. *lupulus*	leaf	DRR024457-DRR024463 / LA368958, LA349193, LA335829, LA337990, LA347589[(10)]
Literature search	(Bester and Maree 2023); South Africa	Viridiplantae / Rosaceae	*Prunus armeniaca*	leaf petiole	MT900926-MT900928
	(Mahlanza et al. 2022); South Africa	Viridiplantae / Solanaceae	*Solanum chenopodioides*	leaf	SRR15040766[g]
	(Dias et al. 2022); Tennessee, USA	Viridiplantae/ Rosaceae	*Prunus persica*	leaf	OL800565-OL800567[g,(25)]
	(Orfanidou et al. 2022); Greece	Viridiplantae/ Solanaceae	*Capsicum annuum**	fruit	OP066714-OP066716[g,(4)]

Serratus-palmID SRA search	(Howe et al. 2023); Michigan, USA	Viridiplantae / Poaceae	*Panicum virgatum* or *Miscanthus* sp. (phyllosphere metatranscriptome)	leaf surface wash / phyllo-sphere RNA	SRR10376089, SRR10376090, SRR10376182-SRR10376185, SRR10376270, SRR10376303, SRR10376306, SRR10376309, SRR10376310, SRR10848930, SRR10848974, SRR10849010-SRR10849012, SRR10849023-SRR10849025, SRR10849154-SRR10849161, SRR10849187, SRR10849194, SRR10849299, SRR10849305, SRR10849306, SRR10849310, SRR11061001, SRR11061006, SRR11061008, SRR11061009, SRR9003207, SRR9003208
	(Auber et al. 2020); Indiana, USA	Viridiplantae / Boraginaceae	*Lithospermum erythrorhizon*	root	SRR10758280, SRR10758281, SRR10758283, SRR10758284, SRR10758308-SRR10758313
	(Arnoux 2019); France	Viridiplantae / Solanaceae	*Capsicum annuum* var. *glabriusculum*	leaf and flower	ERR2576961
	(Haselmair-Gosch et al. 2018); Austria	Viridiplantae / Solanaceae	*Petunia x hybrida*	flower	SRR11808665
	(Rai et al. 2018); Japan	Viridiplantae / Boraginaceae	*Lithospermum officinale*	leaf	SRR6799516-SRR6799518
	(Wu et al. 2018); Venezuela	Viridiplantae / Solanaceae	*Jaltomata repandidentata*	flower	SRR5380917, SRR5380918
	(Chen et al. 2016); China	Viridiplantae / Fabaceae	*Arachis hypogaea*	whole pod	SRR6387685
	(Roux et al. 2014); France	Viridiplantae / Fabaceae	*Medicago truncatula*	root nodule	SRR949232
	(Tauber et al. 2022); Michigan, USA	Animalia / Apidae	*Apis mellifera*	adult bee intestine	SRR12659856
	(Sproviero et al. 2021); Italy	Animalia / Hominidae	*Homo sapiens*	blood plasma	SRR12387953
	(Coady et al. 2020); Michigan, USA	Animalia / Daphniidae	*Daphnia magna*	whole daphnid	SRR11680723
	(Costa et al. 2020); California, USA	Animalia / Apidae	*Bombus impatiens*	whole abdomen	SRR11881307, SRR11881356
	(Deboutte et al. 2020); Belgium	Animalia / Apidae	*A. mellifera*	whole honeybee	SRR10418310
	(Ledón-Rettig et al. 2017); Indiana, USA	Animalia / Scarabaeidae	*Onthophagus taurus*	whole beetle	SRR4412518, SRR4412519
	(Vannette et al. 2015); California, USA	Animalia / Apidae	*A. mellifera*	midgut	SRR1239309

[a] High-throughput sequencing (HTS)-based detections validated by RT-PCR are marked by an asterisk (*) after the plant species name.

[b] SRA datasets where SnIV1 sequences are detected and assembled, and/or GenBank accessions of SnIV1 genomes with number superscripts in parentheses that correspond to each SnIV1 RNA 3 segment that were used in the phylogenetic analyses with the resulting tree shown in Fig. 1 and Supplementary Fig. 2C.

[c] The three genome segments from this study were used as query search for BLASTn searches in GenBank databases.
[d] The virus was deposited under the name 'surrounding legume associated ilarvirus (sLaIV)', and identified from a composite sample of pooled RNAs from three different *Trifolium* species and one *Vicia* species. (see Gaafar et al. 2020 for details).
[e] The virus was deposited under the name 'grapevine associated ilarvirus (GaIV)' and identified from grapevines infected with the downy mildew fungi *Plasmopara viticola* (kingdom *Chromista* / family Peronosporaceae).
[f] The virus was deposited under the name 'Erysiphe necator associated ilar-like virus 1 (EnaIV1)', and identified from grapevines infected with the powdery mildew fungi *Erysiphe necator* (kingdom *Fungi* / family Erysiphaceae).
[g] SnIV1 sequences are not available in GenBank r.v. 250. SnIV1 genomes were either provided upon request from the authors ahead of release or were assembled from the SRA dataset of the study.

Literature Cited within Supplementary Materials

Altschul, S. F., Madden, T. L., Schäffer, A. A., Zhang, J., Zhang, Z., Miller, W., et al. 1997. Gapped BLAST and PSI-BLAST: a new generation of protein database search programs. Nucleic Acids Research. 25:3389–3402.

Arnoux, S. 2019. Comparative analyses of the molecular footprint of domestication in three Solanaceae species: eggplant, pepper and tomato (PhD Thesis). Available at: https://tel.archives-ouvertes.fr/tel-02185095v2/document.

Auber, R. P., Suttiyut, T., McCoy, R. M., Ghaste, M., Crook, J. W., Pendleton, A. L., et al. 2020. Hybrid de novo genome assembly of red gromwell (Lithospermum erythrorhizon) reveals evolutionary insight into shikonin biosynthesis. Horticulture Research. 7:82.

Babaian, A., and Edgar, R. 2022. Ribovirus classification by a polymerase barcode sequence. PeerJ. 10:e14055.

Bester, R., and Maree, H. J. 2023. First report of the plum marbling disease associated agent, plum viroid I, in apricots (Prunus armeniaca) in South Africa. Plant Disease. Available at: https://apsjournals.apsnet.org/doi/10.1094/PDIS-10-22-2321-PDN.

Bouckaert, R., Vaughan, T. G., Barido-Sottani, J., Duchêne, S., Fourment, M., Gavryushkina, A., et al. 2019. BEAST 2.5: An advanced software platform for Bayesian evolutionary analysis. PLoS Computational Biology. 15:e1006650.

Buzkan, N., Chiumenti, M., Massart, S., Sarpkaya, K., Karadağ, S., and Minafra, A. 2019. A new emaravirus discovered in Pistacia from Turkey. Virus Research. 263:159–163.

Chang, S., Puryear, J., and Cairney, J. 1993. A simple and efficient method for isolating RNA from pine trees. Plant Mol Biol Rep. 11:113–116.

Chen, X., Yang, Q., Li, H., Li, H., Hong, Y., Pan, L., et al. 2016. Transcriptome-wide sequencing provides insights into geocarpy in peanut (Arachis hypogaea L.). Plant Biotechnology Journal. 14:1215–1224.

Chiapello, M., Rodriguez-Romero, J., Ayllon, M., and Turina, M. 2019. A report on the virome of obligatory biotrophs. Available at: https://ec.europa.eu/research/participants/documents/downloadPublic?documentIds=080166e5c8e77dab&appId=PPGMS [Accessed February 7, 2022].

Chiapello, M., Rodríguez-Romero, J., Nerva, L., Forgia, M., Chitarra, W., Ayllón, M. A., et al. 2020. Putative new plant viruses associated with Plasmopara viticola -infected grapevine samples. Annals of Applied Biology. 176:180–191.

Coady, K. K., Burgoon, L., Doskey, C., and Davis, J. W. 2020. Assessment of Transcriptomic and Apical Responses of Daphnia magna Exposed to a Polyethylene Microplastic in a 21-d Chronic Study. Environmental Toxicology and Chemistry. 39:1578–1589.

Costa, C. P., Duennes, M. A., Fisher, K., Der, J. P., Watrous, K. M., Okamoto, N., et al. 2020. Transcriptome analysis reveals nutrition- and age-related patterns of gene expression in the fat body of pre-overwintering bumble bee queens. Molecular Ecology. 29:720–737.

Deboutte, W., Beller, L., Yinda, C. K., Maes, P., de Graaf, D. C., and Matthijnssens, J. 2020. Honey-bee–associated prokaryotic viral communities reveal wide viral diversity and a profound metabolic coding potential. Proceedings of the National Academy of Sciences. 117:10511–10519.

Dias, N. P., Hu, R., Hensley, D. D., Hansen, Z. R., Domier, L. L., and Hajimorad, M. R. 2022. A Survey for Viruses and Viroids of Peach in Tennessee Orchards by RNA Sequencing. Plant Health Progress. 23:265–268.

Edgar, R. C., Taylor, J., Lin, V., Altman, T., Barbera, P., Meleshko, D., et al. 2022. Petabase-scale sequence alignment catalyses viral discovery. Nature. 602:142–147.

Gaafar, Y. Z. A., Herz, K., Hartrick, J., Fletcher, J., Blouin, A. G., MacDiarmid, R., et al. 2020. Investigating the Pea Virome in Germany—Old Friends and New Players in the Field(s). Frontiers in Microbiology. 11:2605.

Haselmair-Gosch, C., Miosic, S., Nitarska, D., Roth, B. L., Walliser, B., Paltram, R., et al. 2018. Great Cause—Small Effect: Undeclared Genetically Engineered Orange Petunias Harbor an Inefficient Dihydroflavonol 4-Reductase. Frontiers in Plant Science. 9:149.

Howe, A., Stopnisek, N., Dooley, S. K., Yang, F., Grady, K. L., and Shade, A. 2023. Seasonal activities of the phyllosphere microbiome of perennial crops. Nature Communications. 14:1039.

Illumina. 2023. Sequencing Coverage for NGS Experiments. Available at: https://www.illumina.com/science/technology/next-generation-sequencing/plan-experiments/coverage.html [Accessed April 29, 2023].

Ledón-Rettig, C. C., Zattara, E. E., and Moczek, A. P. 2017. Asymmetric interactions between doublesex and tissue- and sex-specific target genes mediate sexual dimorphism in beetles. Nature Communications. 8:14593.

Li, H. 2018. Minimap2: pairwise alignment for nucleotide sequences. Bioinformatics. 34:3094–3100.

Ma, Y., Marais, A., Lefebvre, M., Faure, C., and Candresse, T. 2020. Metagenomic analysis of virome cross-talk between cultivated Solanum lycopersicum and wild Solanum nigrum. Virology. 540:38–44.

Mahlanza, T., Pierneef, R. E., Makwarela, L., Roberts, R., and van der Merwe, M. 2022. Metagenomic analysis for detection and discovery of plant viruses in wild Solanum spp. in South Africa. Plant Pathology. 71:1633–1644.

Mistry, J., Chuguransky, S., Williams, L., Qureshi, M., Salazar, G. A., Sonnhammer, E. L. L., et al. 2021. Pfam: The protein families database in 2021. Nucleic Acids Research. 49:D412–D419.

Natsume, S., Takagi, H., Shiraishi, A., Murata, J., Toyonaga, H., Patzak, J., et al. 2015. The Draft Genome of Hop (Humulus lupulus), an Essence for Brewing. Plant and Cell Physiology. 56:428–441.

Orfanidou, C. G., Katiou, D., Papadopoulou, E., Katis, N. I., and Maliogka, V. I. 2022. A known ilarvirus is associated with a novel viral disease in pepper. Plant Pathology. 71:1901–1909.

Pecman, A., Adams, I., Gutiérrez-Aguirre, I., Fox, A., Boonham, N., Ravnikar, M., et al. 2022. Systematic Comparison of Nanopore and Illumina Sequencing for the Detection of Plant Viruses and Viroids Using Total RNA Sequencing Approach. Frontiers in Microbiology. 13:1424.

Pecman, A., Kutnjak, D., Gutiérrez-Aguirre, I., Adams, I., Fox, A., Boonham, N., et al. 2017. Next Generation Sequencing for Detection and Discovery of Plant Viruses and Viroids: Comparison of Two Approaches. Frontiers in Microbiology. 8:1–10.

Rai, A., Nakaya, T., Shimizu, Y., Rai, M., Nakamura, M., Suzuki, H., et al. 2018. De Novo Transcriptome Assembly and Characterization of Lithospermum officinale to Discover Putative Genes Involved in Specialized Metabolites Biosynthesis. Planta Medica. 84:920–934.

Rivarez, M. P. S., Pecman, A., Bačnik, K., Maksimović, O., Vučurović, A., Seljak, G., et al. 2023. In-depth study of tomato and weed viromes reveals undiscovered plant virus diversity in an agroecosystem. Microbiome. 11:60.

Roux, B., Rodde, N., Jardinaud, M.-F., Timmers, T., Sauviac, L., Cottret, L., et al. 2014. An integrated analysis of plant and bacterial gene expression in symbiotic root nodules using laser-capture microdissection coupled to RNA sequencing. The Plant Journal. 77:817–837.

Roux, S., Adriaenssens, E. M., Dutilh, B. E., Koonin, E. V., Kropinski, A. M., Krupovic, M., et al. 2019. Minimum Information about an Uncultivated Virus Genome (MIUViG). Nature Biotechnology. 37:29–37.

Sayers, E. W., Bolton, E. E., Brister, J. R., Canese, K., Chan, J., Comeau, D. C., et al. 2022. Database resources of the national center for biotechnology information. Nucleic Acids Research. 50:D20–D26.

Simmonds, P., Adams, M. J., Benkő, M., Breitbart, M., Brister, J. R., Carstens, E. B., et al. 2017. Virus taxonomy in the age of metagenomics. Nature Reviews Microbiology. 15:161–168.

Sproviero, D., Gagliardi, S., Zucca, S., Arigoni, M., Giannini, M., Garofalo, M., et al. 2021. Different miRNA Profiles in Plasma Derived Small and Large Extracellular Vesicles from Patients with Neurodegenerative Diseases. International Journal of Molecular Sciences. 22:2737.

Tauber, J. P., McMahon, D., Ryabov, E. V., Kunat, M., Ptaszyńska, A. A., and Evans, J. D. 2022. Honeybee intestines retain low yeast titers, but no bacterial mutualists, at emergence. Yeast. 39:95–107.

Vannette, R. L., Mohamed, A., and Johnson, B. R. 2015. Forager bees (Apis mellifera) highly express immune and detoxification genes in tissues associated with nectar processing. Scientific Reports. 5:16224.

Wu, M., Kostyun, J. L., Hahn, M. W., and Moyle, L. C. 2018. Dissecting the basis of novel trait evolution in a radiation with widespread phylogenetic discordance. Molecular Ecology. 27:3301–3316.

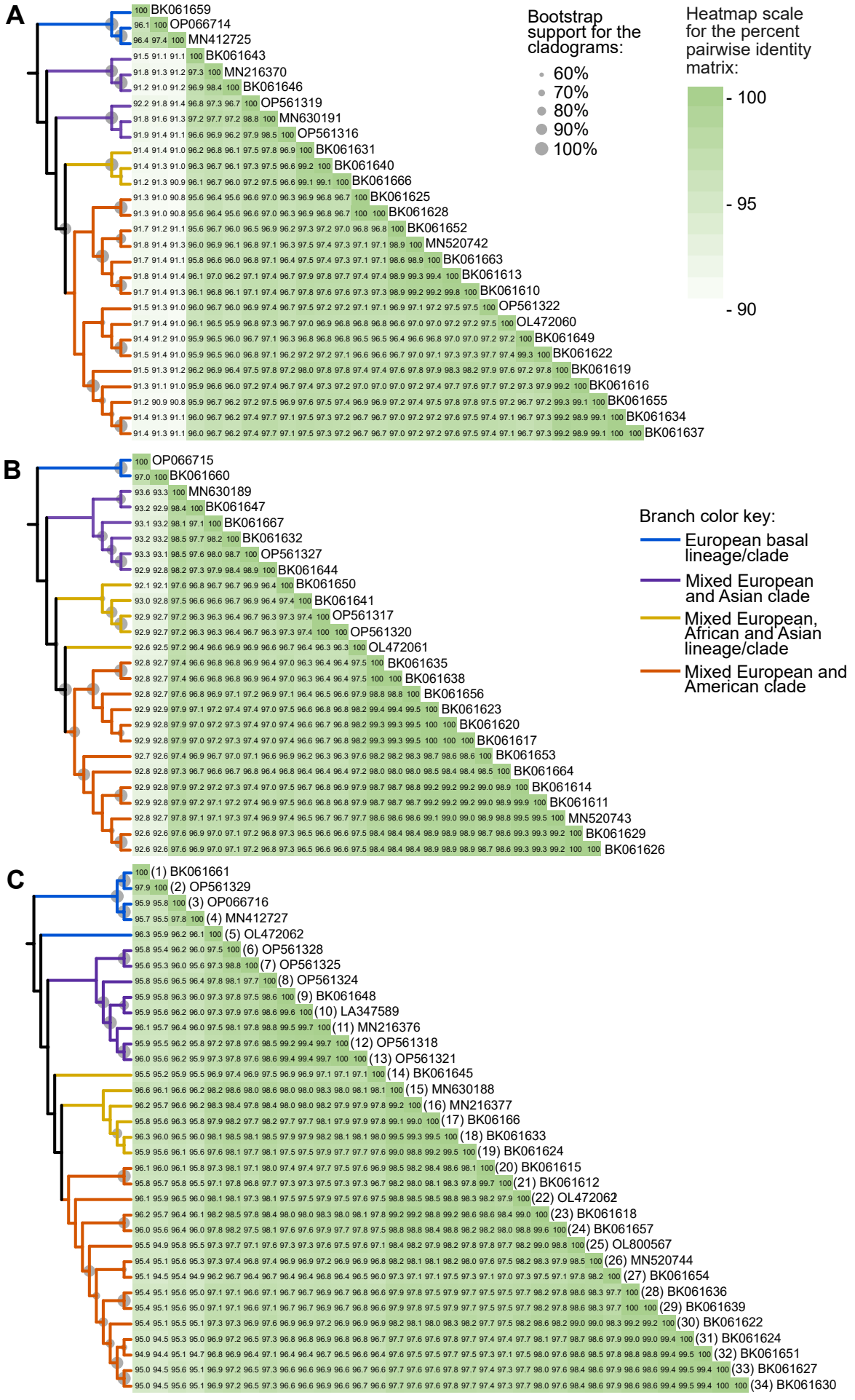

Supplementary Figure 1. Percent pairwise identity among global SnIV1 isolates with their phylogenetic clustering, based on A, RNA 1 (1a open reading frame (ORF)), B, RNA 2 (2a and 2b overlapping ORFs), C, RNA 3 (3a and 3b concatenated ORFs). The maximum likelihood phylogenetic trees were constructed based on the multiple sequence alignments of the aforementioned ORFs and were shown as consensus trees (cladograms). The substitution model used was Tamura 3-parameter with discrete Gamma distribution with 5 rate categories and by assuming that a certain fraction of sites is evolutionarily invariable. The tree topology shown was inferred after 1000 bootstrap replicates. The nucleotide pairwise identity was likewise calculated using the same alignments and are presented as a heatmap. Associated metadata of each sequence used in this analysis can be found in Table 1 and Supplementary Table 2.

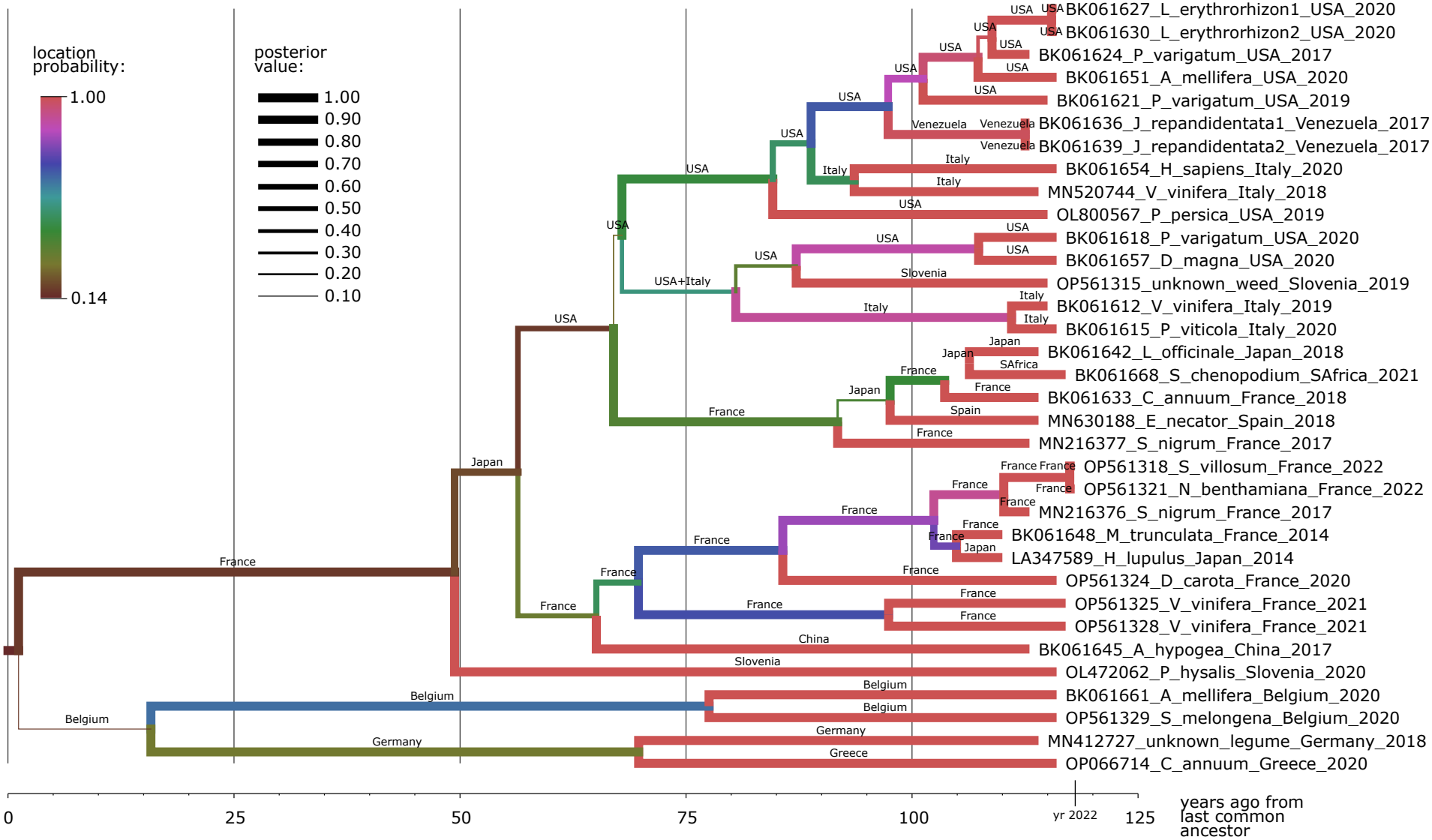

Supplementary Figure 2. Ancestral reconstruction and discrete phylogeography of SnIV1 based on the Bayesian framework. The phylogeographic tree was inferred using the concatenated alignments of the CP and MP (RNA3) coding sequences of 34 global isolates of SnIV1. Branches are colored based on probability of the predicted location, while branch thickness is based on posterior value. The tree is time-scaled by number of years. Parameters on the BEAST v. 2.7.4 analyses were based on the procedure presented in http://beast2-dev.github.io/beast-docs/beast2/PhylogeographyDiscrete/AR.html, with concepts described in Bouckaert et al. 2019 (https://journals.plos.org/ploscompbiol/article?id=10.1371/journal.pcbi.1006650).